ORGANOMETALLICS

pubs.acs.org/Organometallics Article

Diruthenium Complexes with π-Extended Bridging Bis(alkenyl)arylene Ligands, A Derived Metallamacrocycle, and Their Oxidized Forms

Franciska S. Gogesch, Sebastian Schwab, Anja Rehse, Michael Linseis, Ananya Baksi, Guido H. Clever, and Rainer F. Winter*

Cite This: *Organometallics* 2023, 42, 3085−3098

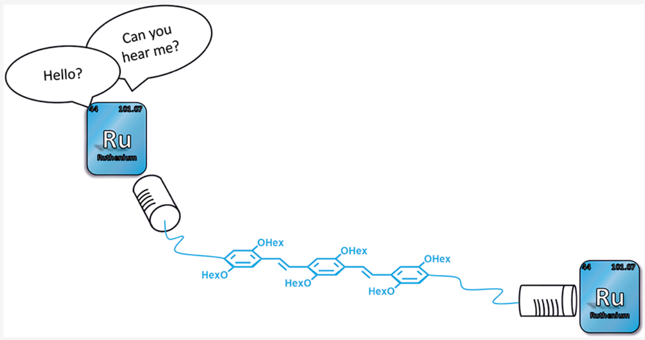

ABSTRACT: We report on dinuclear alkenylruthenium complexes with π-extended *trans,trans*-distyrylbenzene (**1-V**) or 1,4-(2-phenylethynyl)benzene (**1-A**) linkers akin to oligophenylvinylene and oligophenylethynylene oligomers (OPV-3 and OPE-3, respectively) and the macrocylic analogue **2-A**. All compounds were characterized by NMR spectroscopy and high-resolution ESI-MS. Their electrochemical and spectroscopic properties were examined. The efficacy of intramolecular through-bond electron transfer in their mixed-valent, one-electron-oxidized radical cations was probed by UV/vis/NIR and EPR spectroscopy as well as by density functional theory calculations. The terminally appended diruthenium tags of the present compounds add IR spectroscopy to the available toolbox and provide resolved hyperfine splittings to the ^{31}P nuclei in the EPR spectra of their one- and two-electron-oxidized radical cations and dications. Our results indicate charge localization on one {Ru}−CH=CHAr site on the IR time scale for [**1-A**]$^{\bullet+}$ and [**2-A**]$^{\bullet\bullet 2+}$ and a small degree of charge delocalization in [**1-V**]$^{\bullet+}$. On the slower time scale of EPR spectroscopy, [**1-V**]$^{\bullet+}$ and [**1-A**]$^{\bullet+}$ become valence-detrapped or nearly so. The near breakdown of electronic coupling on fast time scales is also indicated by the finding that the chromophores present in [**1-V**]$^{\bullet+}$ and [**1-V**]$^{2+}$, in [**1-A**]$^{\bullet+}$ and [**1-A**]$^{2+}$, and in [**2-A**]$^{\bullet\bullet 2+}$ and [**2-A**]$^{4+}$ are mutually identical.

■ INTRODUCTION

Bis(alkenyl)arylene-bridged diruthenium complexes of the type [{Ru}$_2$(μ-CH=CH−arylene−CH=CH)] ({Ru} = Ru(CO)(PR$_3$)$_2$(L)(X); X = monodenate anionic ligand, L = PR$_3$ or a vacant coordination site; or (L)(X) = bidentate monoanionic carboxylate or β-keto enolate ligand) usually undergo two consecutive one-electron oxidations due to the inherent redox activity of the {Ru}−CH=CHR entities, thus offering at least three individually accessible oxidation states. Additional ones may ensue, if the bridging arylene ligand is redox-active by itself.[1−21] Strong absorption of the oxidized states in the visible (vis) and near-infrared (NIR) is an attractive feature of such complexes. They are tokens of bridge contributions to the individual redox processes, which render the bridging divinylarylene ligand redox-noninnocent. It is therefore only natural that the half-wave potential splitting $\Delta E_{1/2}$ between adjacent redox waves, e.g., $\Delta E_{1/2} = E_{1/2}^{+/2+} - E_{1/2}^{0/+}$, depends strongly on the identity and the electronic properties of the bridging arylene ligand.

As a result of sizable bridge contributions to the frontier molecular orbitals (MOs), a surprisingly large extent of charge and spin delocalization in the one-electron-oxidized mixed-valent (MV) states of these complexes is often observed despite rather small values of $\Delta E_{1/2}$. Electronic coupling between the two individual vinylruthenium halves of such molecules is nevertheless attenuated as the length of the bridging ligand increases. As an example, the MV one-electron-oxidized form of the 1,4-divinylphenylene-bridged complex **1-P** in Figure 1, whose $\Delta E_{1/2}$ is 250 mV,[22] displays full charge and spin delocalization on the time scale of IR and EPR spectroscopy and hence constitutes a Class III mixed-valent system according to the classification scheme of Robin and Day.[23] In the stilbenyl-bridged complex **1-S**, $\Delta E_{1/2}$ is decreased to 49 mV. The radical cation [**1-S**]$^{\bullet+}$ is a localized MV system of Class II on the time scale of IR spectroscopy (ca. 5 × 10^{-11} s).[4] The corresponding charge distribution parameter, which is based on energy shifts of the charge-sensitive stretching vibrations of carbonyl ligands as a response to stepwise oxidations, provides a quantitative measure

Received: July 28, 2023
Revised: October 9, 2023
Accepted: October 10, 2023
Published: October 27, 2023

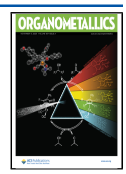

https://doi.org/10.1021/acs.organomet.3c00337
Organometallics 2023, 42, 3085−3098

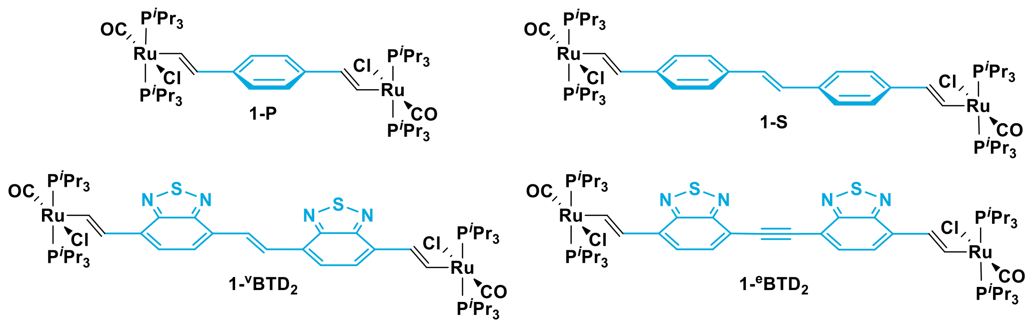

Figure 1. Chemical structures of bis(alkenyl)arylene-bridged diruthenium complexes that are relevant for the present work.

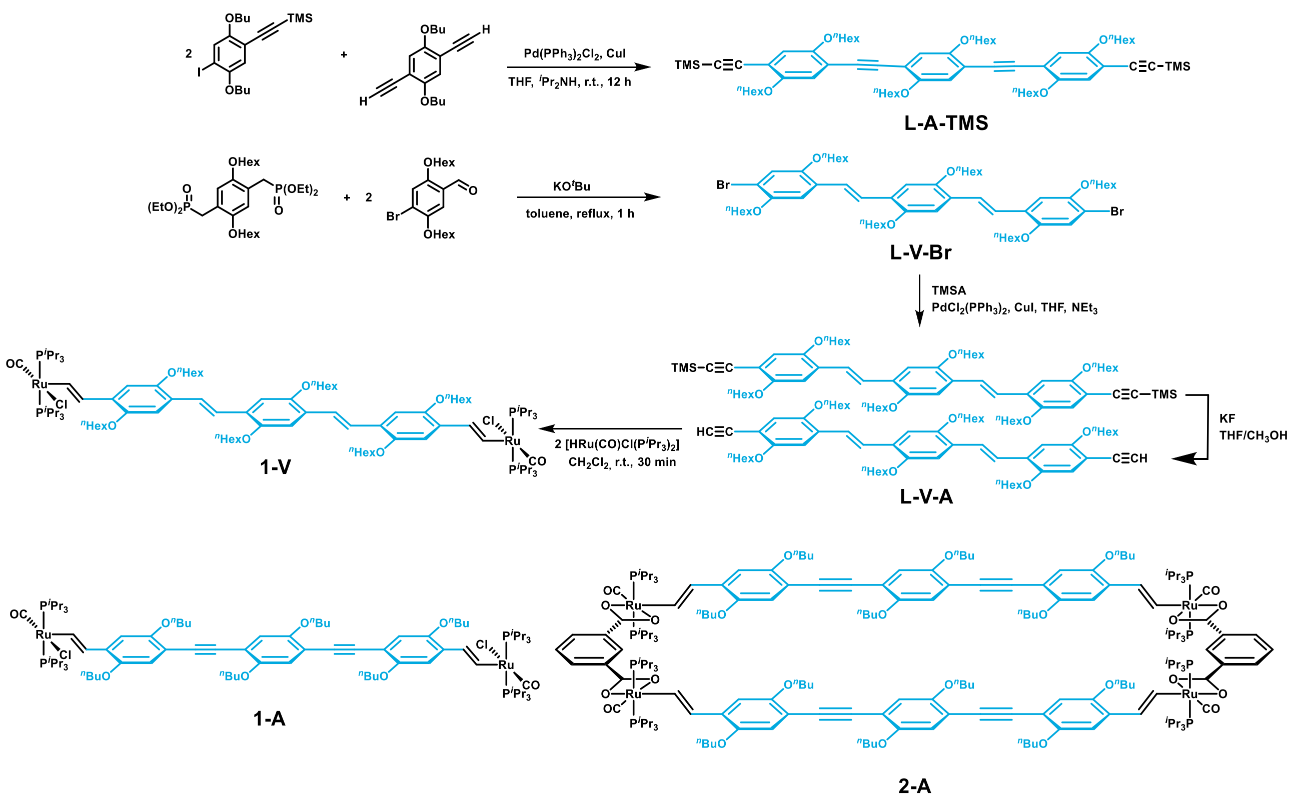

Figure 2. Synthesis of the ligand precursors and structures of diruthenium complexes **1-V** and **1-A** and of the tetraruthenium metallamacrocycle **2-A** (TMSA = trimethylsilylacetylene, TMS = trimethylsilyl).

of the extent to which the electron hole is shared by the two molecular halves.[24,25] A value $\Delta\rho = 0.19$ for $[\mathbf{1\text{-}S}]^{\bullet+}$ signals that in the electronic ground state, ca. 81% of the unipositive charge resides on one styryl ruthenium entity and the remaining 19% on the other.[4] This value is unexpectedly large if one considers the small redox splitting. Moreover, on the slower time scale of EPR spectroscopy (ca. 10^{-8} s), the spin density is fully delocalized, as indicated by identical hyperfine splittings to the ^{31}P nuclei of four P^{i}Pr$_3$ ligands and two $^{99/101}$Ru nuclei each.[3] Complexes **1-^{E}BTD$_2$** and **1-^{V}BTD$_2$** (Figure 1), with the same molecular linker lengths as **1-S** but attenuated aromaticity of the arylene linkers, show the same general behavior. However, their $\Delta\rho$ values of 0.24 and 0.31, respectively, are larger, despite an even smaller half-wave potential splitting or potential inversion (i.e., a negative value of $\Delta E_{1/2}$).[1]

In our continuous efforts to probe the electron-transfer properties of bis(alkenyl)arylene-bridged diruthenium complexes, we report here on diruthenium complexes with the next higher members of phenylenevinylene and phenyleneethynylene oligomers (OPVs and OPEs, respectively) as the bridging ligands. OPVs and OPEs are paradigmatic examples of oligomers that become electrically conductive upon doping with a suitable oxidant or reductant and are hence dubbed "synthetic metals".[26,27] Their (semi)conducting properties upon doping,[28,29] their wirelike behavior in single-molecule nanoelectrode setups,[30,31] their chemical stability, and their interesting optical and luminescence properties,[32−37] including electroluminescence,[38] are attractive assets. The stiffer rigid-rod structures of ethynylene-bridged poly(phenyleneethynylenes) (PPEs) are often thought to decrease the impact of ring torsions along the π-conjugated backbone.[39−46] The ability of molecule-based wires with varying numbers of identical π-conjugated repeat units in their backbones to transport charge over longer distances can be evaluated by measuring the decay of conductance G as a function of the molecular length L. The latter scales according to

$$G = A\cdot e^{-\beta L} \tag{1}$$

where β is the so-called attenuation factor.[47,48] For OPVs and OPEs, β values for charge transport according to the superexchange mechanism, i.e., through direct orbital interactions, are in the range of 0.14−0.18[30,42,49,50] and 0.20−0.34 $Å^{-1}$,[46,51−53] respectively. Rates of intramolecular electron transfer (k_{ET}) over OPE and OPV linkers were determined by various methods, including variable-temperature EPR spectroscopy on mixed-valent states of appropriately modified congeners[42,54] and energy or electron transfer between terminally appended donors and acceptors in the photoexcited state.[39,50,55,56] The {Ru} end groups used in this study add IR spectroscopy to the portfolio of available methods. Previous studies on the MV radical anions of OPV-bridged bis(perchlorotriphenylmethyl) radicals,[42] radical cations of bis(diarylamine)s,[57,58] and OPV-bridged donor−acceptor dyads[30] showed that the OPV-3 congener with three phenylene-ethenylene repeat units in the linker is close to or at the point where the dominant transport mechanism changes from superexchange to incoherent hopping, as was, e.g., indicated by abrupt changes of the rate constants and slopes when plotting ln k_{ET} as a function of the spatial distance L between the radical centers. This prompted us to extend our previous work on divinylarylene-bridged diruthenium complexes to OPV-3 and blends of OPV-3 and OPE-3 linkers.

■ RESULTS AND DISCUSSION

Synthesis and Characterization. Figure 2 shows the bis(alkenyl)arylene-bridged diruthenium complexes **1-V** and **1-A** of the present study. Their π-extended conjugated backbones consist of three ethenyl- or ethynyl-bridged phenyl rings, which renders **1-V** and **1-A** metal−organic analogs of OPV-3 or an OPE-3/OPV-3 blend. The general synthesis protocol employs twofold hydroruthenation[59] of the corresponding dialkyne precursors **L-V-A** or **L-A-A**, which were generated from their trimethylsilyl (TMS)-protected precursors **L-V-TMS** or **L-A-TMS** by treatment with KF in a THF/MeOH solvent mixture. After workup, complexes **1-V** and **1-A** were obtained as red solids in isolated yields of 50% and 38%, respectively. The macrocyclic complex **2-A** was prepared according to an established procedure[60−62] by adding a methanolic solution of isophthalic acid and potassium carbonate base to a solution containing an equimolar amount of **1-A**. After workup, metallamacrocycle **2-A** was isolated as a red solid in a yield of 27%. Detailed synthesis procedures for the complexes and their bridge precursors, reaction schemes, and characterization data as well as NMR spectra (^{1}H, ^{13}C{^{1}H}, and ^{31}P{^{1}H}), mass spectra, and the results of combustion analyses are provided in the Experimental Section in the Supporting Information (Schemes S1−S3 and Figures S1−S19). Compounds **1-V** and **1-A** are air- and moisture-stable in the solid state as well as in solution, whereas macrocycle **2-A** decomposes within a few hours in solution. Selected NMR data are summarized in Table 1.

Table 1. Selected ^{31}P{^{1}H}, ^{1}H, and ^{13}C{^{1}H} NMR Spectroscopic Data for 1-V, 1-A, and 2-A, Measured in C_6D_6[a]

	P^iPr_3	Ru−C*H* ($^3J_{HH}$)	Ru−CH═C*H* ($^3J_{HH}$)	C_{CO} ($^2J_{CP}$)
1-V	38.65	9.09 (13.4)	6.97 (13.4)	203.4 (13.1)
1-A	38.79	9.18 (13.3)	6.95 (13.3)	203.7 (12.7)
2-A	38.12	9.37 (14.9)	7.27 (−)	209.3 (−)

[a]Chemical shifts δ are given in ppm and coupling constants in Hz.

Both complexes show one sharp singlet resonance in their ^{31}P{^{1}H} NMR spectrum with a chemical shift of δ = 38.65 or 38.79 ppm for complex **1-V** or **1-A**, respectively, with five-coordinate, 16 valence electron (VE) ruthenium moieties. As per usual, a modest shift to higher field (δ = 38.12 ppm) is observed upon coordinative saturation in **2-A**.[60−62] The α and β vinyl protons give rise to characteristic sets of doublet resonances at δ = 9.37−9.09 and 7.27−6.95 ppm, respectively, with more high-field-shifted resonances for **2-A**. The $^3J_{HH}$ coupling constants of 13.3−14.9 Hz are typical for a *trans* stereochemistry at the olefinic double bonds. Upon hydroruthenation, the signals for the protons at the central double bonds of **1-V** are shifted downfield by ca. 0.6 ppm from those of their dialkyne precursor **L-V-TMS** (δ = 7.49 and 7.43 ppm) to 8.07 and 8.00 ppm. Smaller downfield shifts of 0.24−0.49 ppm are noted for the aryl protons. The ^{1}H NMR spectrum of **2-A** shows only one set of resonances for chemically equivalent alkenyl and aryl protons and carbon atoms, with no traces of signals that could be assigned to end groups of a linear oligomer, thereby confirming its cyclic structure.

The carbonyl C atoms of complexes **1-V** and **1-A** give rise to a characteristic triplet resonance at δ = 203.6 and 203.7 ppm with $^2J_{CP}$ coupling constants of 13.1 or 12.7 Hz, respectively. The downfield shift of the ^{13}C{^{1}H} CO resonance of **2-A** to δ = 209.3 ppm agrees with previous observations on similar complexes.[60−62] Identification of **2-A** as a tetranuclear complex rests on the observation of the $[M]^{2+}$ mass peak at 1824.3599 amu (calculated value: 1824.3668) with 0.500 spacings for adjacent isotopomers in ultrahigh-resolution electrospray ionization mass spectrometry (UHR-ESI-MS) (see Figure S5).

In their electronic spectra, **1-V** and **1-A** exhibit a highly intense ($\varepsilon \approx$ 80.000 M^{-1} cm^{-1}) $\pi \rightarrow \pi^*$ transition at 460 and 436 nm, respectively, whose overall appearance resembles that of their alkynyl precursors **L-V-TMS** and **L-A-TMS** (Figures S21 and S22). In **2-A**, the band is located at 441 nm, and its intensity is roughly doubled due to the presence of two identical chromophores of type **1-A** within the same molecule. Comparison with **1-P** (λ_{max} = 353 nm) and **1-S** (λ_{max} = 407 nm) demonstrates the effect of stepwise insertion of styryl or ethynylphenyl repeat units into the bridge. Converting the terminal TMS-protected ethynyl functionalities of precursors **L-V-TMS** (λ_{max} = 430 nm) and **L-A-TMS** (λ_{max} = 402 nm) to vinylruthenium entities extends the π-conjugated chromophore in an equally efficient manner. In fact, **1-V** and **1-A** absorb at even lower energies than comparable dialkoxy-substituted OPV-5 and mixed OPV/OPE derivatives with five repeat units ($\lambda_{max} \approx$ 450 or 426 nm, respectively)[36,63−66] and diarylamine-terminated OPVs of identical spacer length (λ_{max} = 437 nm).[67]

Quantum-chemical calculations on slightly truncated PMe_3 models **1-V^{Me}** and **1-A^{Me}** of the real complexes using density functional theory (DFT) or time-dependent DFT (TD-DFT) at the BLYP35/6-31G(d)PCM($ClCH_2-CH_2Cl$) level[68] (for details, see the Supporting Information) indicate that the relevant frontier MOs are symmetrically delocalized over the entire metal−organic π system, yet with varying contributions from the inner/outer segments of the OPV bridge and the CH═CH−{Ru} end groups. MOs HOMO−3 to LUMO+3 of **1-A^{Me}** are shown in Figure 3, while those of **1-V^{Me}** are depicted in Figure S47. We note an excellent match between computed and experimental spectra (see Figures S48 and S53 for a comparison). The prominent visible band at λ_{calc} = 456 nm for **1-V^{Me}** or 436 nm for **1-A^{Me}** with oscillator strengths (f) greater than 3.1 and the weaker absorptions near 290 nm with $f \approx$ 0.3−

https://doi.org/10.1021/acs.organomet.3c00337
Organometallics 2023, 42, 3085−3098

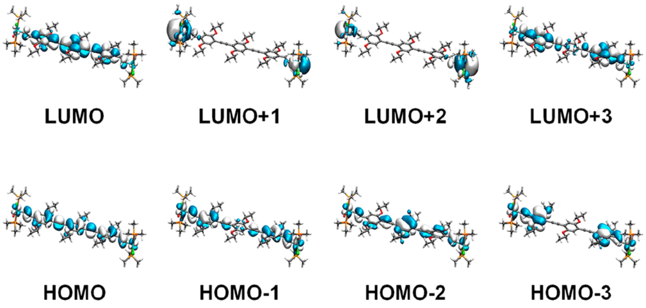

Figure 3. Contour plots of the calculated MOs from HOMO−3 to LUMO+3 of the simplified PMe_3 model **1-A**^{Me} of **1-A** (BLYP35/6-31G(d)PCM($ClCH_2-CH_2Cl$).

0.4 are identified as $\pi \rightarrow \pi^*$ transitions within the extended metal−organic chromophore concomitant with some transfer of electron density from the electron-rich {Ru}−CH═CH− entities to the central phenylene ring.

Electrochemistry and Spectroscopic Studies on the Oxidized Forms. *Electrochemistry.* The redox properties of **1-V**, **1-A**, and **2-A** and the TMS-protected ligand precursors **L-V-TMS** and **L-A-TMS** were investigated by cyclic and square-wave voltammetry. The results are shown in Figures 4 and S23−S29.

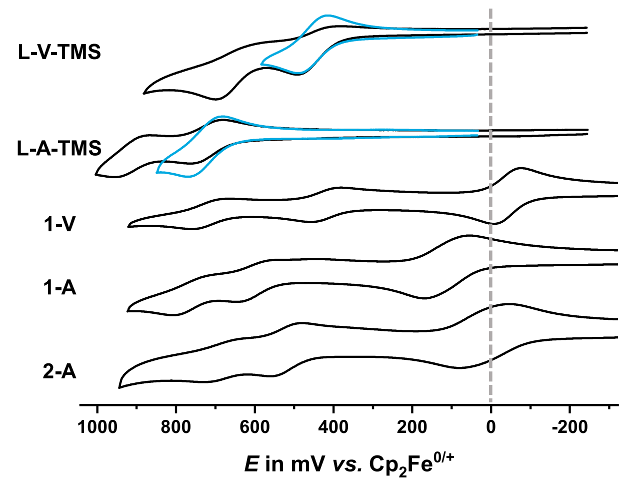

Figure 4. Cyclic voltammograms of **L-V-TMS**, **L-A-TMS**, **1-V**, **1-A**, and **2-A** at ν = 100 mV/s, measured in CH_2Cl_2/0.1 M $^nBu_4N^+PF_6^-$. The dashed gray line at E = 0 mV serves as a guide to the eye.

L-V-TMS and **L-A-TMS** undergo two successive one-electron oxidations with half-wave potential separations $\Delta E_{1/2}$ of 216 and 196 mV, respectively. For both, the first wave has all attributes of chemical and electrochemical reversibility, complying with the requirements of a Nernstian process. The second oxidation of **L-A-TMS** is chemically only partially reversible at low sweep rates (ν) but becomes reversible at a sweep rate of 800 mV/s, whereas even higher sweep rates of up to 1 V/s do not suffice to render this process fully reversible for **L-V-TMS** (see Figures S23 and S24). Although only differing in the order of the C−C bonds that link the phenyl rings, **L-V-TMS** oxidizes at 290 ($E_{1/2}^{0/+}$) or 270 mV ($E_{1/2}^{+/2+}$) lower potential than **L-A-TMS**. This result agrees with the positive value of the Hammett parameter of an alkynyl substituent (σ_p = 0.23) compared to the slightly negative one of a vinyl substituent (σ_p = −0.04),[69] so that the oxidation potentials of such oligomers generally increase with a larger number of triple bonds within the main chain.[31,41,64,65,70−73]

The derived diruthenium complexes **1-V** and **1-A** display a pattern of one two-electron oxidation followed by two additional, well-separated one-electron oxidations. The assignment of the first wave as an overall two-electron process comprising two merged one-electron oxidations rests on the comparison of associated peak currents. For **1-V**, all of the oxidation processes are chemically reversible (Figure S27). However, the fourth oxidation of **1-A** achieves only partial chemical reversibility, even at a sweep rate of 1 V/s (Figure S28). The number of electrons involved in every oxidation process doubles in metallamacrocycle **2-A**, where two identical, mutually insulated **1-A** subunits are present. Hence, **2-A** shows one reversible overall four-electron oxidation plus two additional two-electron oxidations with improved chemical reversibility compared to **1-A** (Figure S29). The merged one-electron oxidations in **1-A**, **1-V**, and **2-A** required digital deconvolution of square-wave voltammograms or, in the case of **1-V**, digital simulation of cyclic voltammograms[74,75] (see Figures S25 and S26) in order to determine the individual half-wave potentials $E_{1/2}^{0/+}$ and $E_{1/2}^{+/2+}$. The corresponding values are listed in Table 2;

Table 2. Half-Wave Potentials of Dinuclear Complexes 1-V and 1-A and of Macrocyclic Complex 2-A in mV vs $Cp_2Fe^{0/+}$, Measured in 0.1 M CH_2Cl_2/$^nBu_4N^+PF_6^-$ at Room Temperature[a]

	$E_{1/2}^{ox1}$	$E_{1/2}^{ox2}$	$E_{1/2}^{ox3}$	$E_{1/2}^{ox4}$
1-V	−61	−21	398	698
1-A	86	144	600	764
2-A[a]	−32	36	519	683
L-V-TMS	446	662		
L-A-TMS	736	932		

[a]The number of transferred electrons is 1 for each step in the dinuclear complexes and 2 for tetranuclear **2-A**.

those of the higher oxidations could directly be determined from the average potentials of the forward and reverse peaks in the cyclic voltammograms and the peak positions in the square-wave voltammograms.

Comparison of the half-wave potentials in Table 2 reveals the following: (i) As for their ligand precursors, all oxidation processes shift to more positive values when the central vinylene linkers of **1-V** are replaced by alkynylene ones in **1-A**. This concurs with the more electron-withdrawing character of an alkynyl group compared to a vinyl group.[1,49,69,76] (ii) The magnitude of the shift is attenuated compared to **L-V-TMS** and **L-A-TMS**. (iii) The alkenylruthenium end groups cause massive shifts of the first three or even all four oxidations to more negative potentials compared to the TMS-protected alkynes. (iv) Coordinative saturation of the ruthenium termini in **2-A** displaces all redox potentials to more negative values with respect to **1-A**. The half-wave potential shifts between **2-A** and **1-A** are nevertheless smaller than those of ca. 200 mV for previously reported pairs of 16 VE dinuclear and cyclic tetranuclear bis(alkenyl)ruthenium 18 VE complexes.[5,61,77,78] This points to lower metal and enhanced bridge contributions to individual oxidations. (v) The differences in half-wave potentials of equivalent redox processes of **1-A**, **2-A**, and **1-V** decrease as the overall oxidation state increases. (vi) The pattern of two nearly coincident one-electron waves at low potential and two separate one-electron oxidations at higher potentials that

https://doi.org/10.1021/acs.organomet.3c00337
Organometallics 2023, 42, 3085−3098

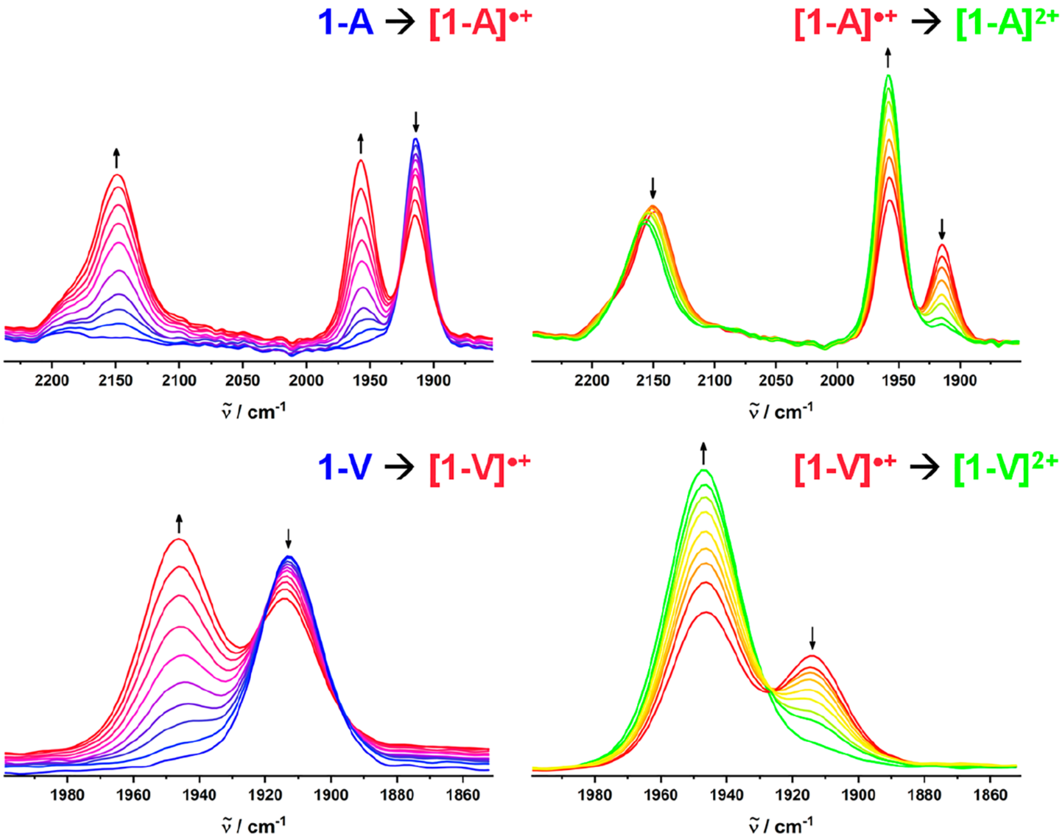

Figure 5. Changes in IR spectra (range of the CO and alkynyl CC stretches) upon the stepwise oxidation of (top) **1-A** and (bottom) **1-V**, measured in 1,2-$C_2H_4Cl_2$/$^nBu_4N^+PF_6^-$.

resemble those of the ligand precursors **L-V-TMS** and **L-A-TMS** suggests an oxidation sequence where the outer styrylruthenium entities are oxidized first, followed by two further oxidations of the π-conjugated linker. OPVs with larger numbers of repeat units within the π-conjugated chain also exhibit a trend toward the gradual merging of the first two one-electron redox waves to a two-electron process with a concomitant lowering in oxidation potentials and the emergence of additional higher oxidations.[65,79,80] (vii) For both **1-V** and **1-A**, the two one-electron oxidations that underlie the composite two-electron wave are separated by only 40 or 58 mV, respectively.

According to eqs 2 and 3, the comproportionation constant K_c for the chemical equilibrium between the monocations on the one hand and the neutral and dicationic forms on the other amounts to only 5 for **1-V** and to 10 for **1-A**. This translates into an equilibrium composition of 52% of the one-electron-oxidized form besides 24% of the neutral and the dioxidized forms each for **1-V**, and of 60% of the one-electron-oxidized form besides 20% of the neutral and the dioxidized forms each for **1-A** after stoichiometric release of one electron from the dinuclear complexes.

$$K_c = \exp\left[\frac{F}{RT}(E_{1/2}^{+/2+} - E_{1/2}^{0/+})\right] = \exp\left(\frac{F\Delta E_{1/2}}{RT}\right) \quad (2)$$

$$K_c = \frac{[A^{\bullet+}]^2}{[A^{2+}][A]} \quad (3)$$

where R is the universal gas constant, F is Faraday's constant, and $[A^{n+}]$ denotes the concentration of the compound in question in its corresponding oxidation state.

Delocalization and Electronic Structure as Probed by IR/NIR and UV/Vis/NIR Spectroscopy. Key to the present study are the questions of bridge versus {Ru} end group contributions to the individual redox processes and the degree of electronic coupling in the one-electron-oxidized MV states. Both these issues can be addressed by analyzing the oxidation-induced shifts and ensuing patterns of CO stretching vibrations of the carbonyl ligands at the {Ru} termini as well as the hyperfine splitting (hfs) constants $A(^{31}P)$ and $A(^{99/101}Ru)$ to the phosphorus and the ruthenium nuclei in EPR spectra. In order to generate the various oxidized forms, we resorted to a combined approach of spectroelectrochemistry (SEC), i.e., the electrochemical oxidation of the complexes inside a thin-layer electrolysis cell equipped with optically and IR transparent CaF_2 windows under simultaneous monitoring of their spectra,[81] and chemical oxidation with an appropriate, selective oxidant.[82] The latter studies confirmed the two- or four-electron nature of the first oxidation wave in complexes **1-V**, **1-A**, and **2-A**. As spectroelectrochemical measurements require significantly longer time scales than cyclic or square-wave voltammetry, these studies provide additional information on the chemical stability of the oxidized complexes.

Figure 5 shows the results of SEC studies of **1-A** and **1-V** in the mid-IR region; IR/NIR spectra and the results of IR/NIR SEC experiments on **2-A** are depicted in Figures S30−S32. Relevant data are collected in Tables 3 and S1. For both compounds, clean isosbestic points were observed throughout the entire two-electron oxidation, and rereduction of the so-obtained solutions restored the original spectra in nearly quantitative spectroscopic yields.

https://doi.org/10.1021/acs.organomet.3c00337
Organometallics 2023, 42, 3085−3098

Table 3. Characteristic Spectroscopic Data for Diruthenium Complexes 1-V and 1-A and Macrocyclic Complex 2-A in All Accessible Oxidation States, Measured in $C_2H_4Cl_2/^nBu_4N^+PF_6^-$

	$\tilde{\nu}_{CO}$ ($\tilde{\nu}_{C\equiv C}$) (cm^{-1})	λ/nm ($\varepsilon_{max}/10^3\ M^{-1}\ cm^{-1}$)
1-V	1912	460 (80.8)
[**1-V**]$^{\bullet+a}$	1915, 1947	1729 (8.4), 1423 (18.1), 1234 (16.7), 1075 (10.2), 707 (18.1), 450 (30.6)
[**1-V**]$^{\bullet+b,f}$	1923, 1941	2955, 2330, 1865, 1470, 1280, 1110
[**1-V**]$^{\bullet+c,f}$	1921, 1941	2840, 2485, 1995, 1530, 1280, 1110
[**1-V**]$^{\bullet+d,f}$	1914, 1947	2490, 1935, 1345, 1240, 1065
[**1-V**]$^{\bullet+e,f}$	1913, 1947	2460, 1240, 1395, 1240, 1100
[**1-V**]$^{2+}$	1947	1430 (27.5), 1240 (63.3), 1060 (34.2), 611 (15.5), 492 (18.3)
[**1-V**]$^{3+g}$	1966	1255 (29.7), 1255 (55.3), 1104 (44.1), 1020 (29.5), 457 (24.6), 263 (90.9), 229 (137.4)
[**1-V**]$^{4+h}$	1973	–
1-A	1914 (2200)	436 (79.4)
[**1-A**]$^{\bullet+a}$	1915, 1956 (2147)	1826 (2.9), 1370 (7.6), 1164 (9.1), 1012 (3.1), 580 (19.9), 510 (23.8), 396 (21.8)
[**1-A**]$^{\bullet+b,f}$	1914, 1955 (2143)	1180
[**1-A**]$^{\bullet+c,f}$	1914, 1956 (2145)	1180
[**1-A**]$^{2+}$	1959 (2157)	1350 (4.1), 1190 (26.7), 1015 (16.6), 555 (31.2), 488 (37.7)
2-A	1905 (2184)	441 (155.9)
[**2-A**]$^{\bullet\bullet2+a}$	–	1675 (4.9), 1293 (7.0), 1147 (28.8), 1000 (12.6), 582 (50.6), 450 (90.3)
[**2-A**]$^{4+}$	1957 (2162)	1300 (7.2), 1160 (45.7), 1000 (34.4), 558 (65.4), 488 (79.7)

[a]Obtained from analytical reconstruction of the spectrum with consideration of the comproportionation equilibrium. [b]Obtained by chemical oxidation with 0.2 equiv of $FcH^+BArF_{24}^-$. [c]Obtained by chemical oxidation with 0.2 equiv of $FcH^+PF_6^-$. [d]Obtained by chemical oxidation with 0.2 equiv of $FcH^+BArF_{24}^-$ in 0.2 M $^nBu_4N^+BArF_{24}^-$. [e]Obtained by chemical oxidation with 0.2 equiv of $FcH^+BArF_{24}^-$ in 0.2 M $^nBu_4N^+PF_6^-$. [f]λ derived from (deconvolution of) IR/NIR spectra. [g]Obtained by chemical oxidation with 3.2 equiv of diacetylferrocenium hexafluoroantimonate. [h]Obtained by chemical oxidation with 4.2 equiv of thianthrenium hexafluoroantimonate; rapid decomposition impedes proper UV/vis band analysis.

The small values of K_c pose the problem that the neutral, monooxidized, and dioxidized forms of the complexes will coexist in solution until full conversion to the respective dication is achieved. As a result, the peak positions of the CO stretching vibrations of the MV monocations [**1-V**]$^{\bullet+}$ and [**1-A**]$^{\bullet+}$ or dication [**2-A**]$^{\bullet\bullet2+}$ cannot directly be obtained and need to be reconstructed from the experimental spectra. Details of the employed procedure can be found in the Supporting Information. The calculated and deconvoluted spectra are depicted in Figures S37–S39; details of the analysis procedure can be found in the Supporting Information. The applied procedure is concededly only approximate and assumes that the comproportionation equilibrium near the working electrode is fully established, that full conversion to the dicationic form is achieved after electrolysis, and that all species are chemically stable. While the clean isosbestic points and high spectroscopic yields on rereduction indicate that the latter criterion is fulfilled, no full conversion to the dications was possible under the thin-layer conditions because of continued diffusion of unconverted neutral starting material from the surrounding solution to the working electrode. This is evidenced by small peaks in the IR spectra for residual **1-A** and **1-V** (Figure 5). Despite the resulting inaccuracies of this analysis, we deem the results sufficiently reliable for the following discussion.

The spectroscopic Ru(CO) band signatures for equivalent charge states of diruthenium complexes [**1-V**]$^{n+}$ and [**1-A**]$^{n+}$ and of [**2-A**]$^{2n+}$ are nearly identical. Their neutral forms exhibit a single, sharp carbonyl absorption at 1912 or 1913 cm^{-1}; the latter band is red-shifted to 1905 cm^{-1} in coordinatively saturated **2-A**. After net two-/four-electron oxidation, the CO band is found at 1947 ([**1-V**]$^{2+}$), 1959 ([**1-A**]$^{2+}$) or 1957 cm^{-1} ([**2-A**]$^{4+}$). The CO band shifts of only 35 cm^{-1} in **1-V** and 46 cm^{-1} in **1-A** are to be compared to those of ca. 120 cm^{-1} observed for trigonal-bipyramidal five-coordinate Ru carbonyl complexes $[Ru(CO)_3(PR_3)_2]^{0/+}$, where the oxidation is Ru-based.[83] **1-V** thus complements a homologous series of complexes **1-P**, **1-S**, and **1-V**, where the CO band shift on twofold oxidation continuously decreases from 81 to 53 and finally to 35 cm^{-1} as the π-conjugated OPV linker gets longer. The observed trends are tokens of increasing bridge contributions to the HOMO within this series and indicate that the latter are enhanced in **1-V** compared to **1-A** and **2-A**.

The spectra in Figure 5 show that the Ru(CO) bands of the intermediate one-electron-oxidized forms [**1-V**]$^{\bullet+}$ and [**1-A**]$^{\bullet+}$

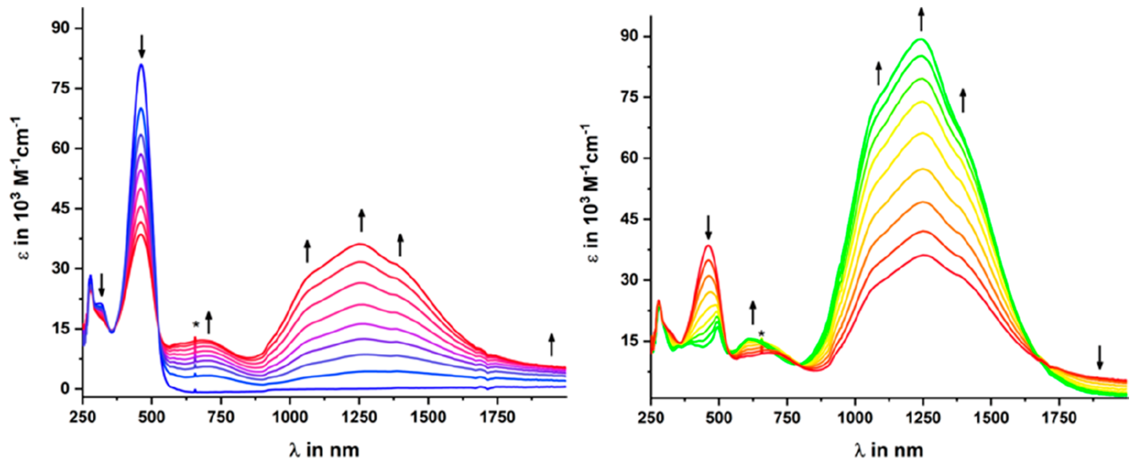

Figure 6. Changes in UV/vis/NIR spectra upon stepwise oxidation of **1-V**, measured in $1,2\text{-}C_2H_4Cl_2/^nBu_4N^+PF_6^-$ (0.2 M) at room temperature.

https://doi.org/10.1021/acs.organomet.3c00337
Organometallics 2023, 42, 3085–3098

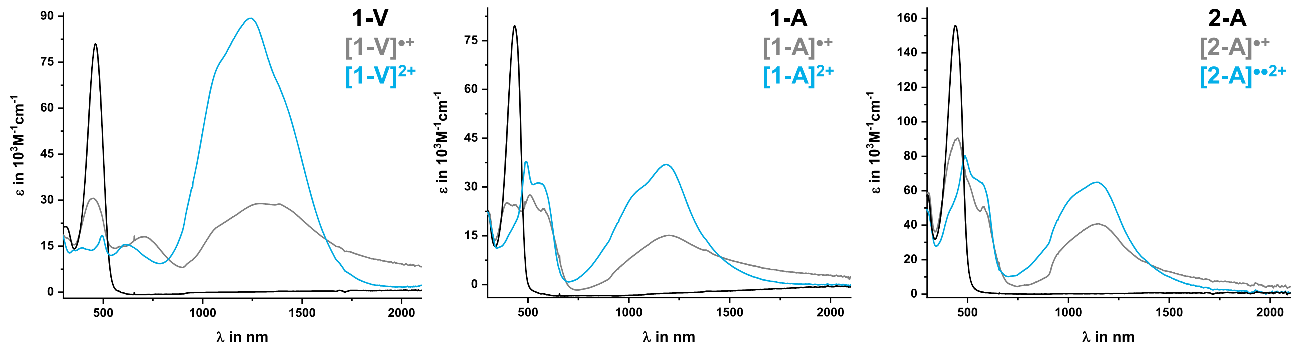

Figure 7. UV/vis/NIR spectra of neutral (black lines), monocationic (gray lines; spectra reconstructed with consideration of the disproportionation equilibrium constant), and dicationic forms (blue lines) of complexes **1-V** (left), **1-A** (middle), and **2-A** (right), measured in 1,2-$C_2H_4Cl_2$/$^nBu_4N^+PF_6^-$ (0.2 M).

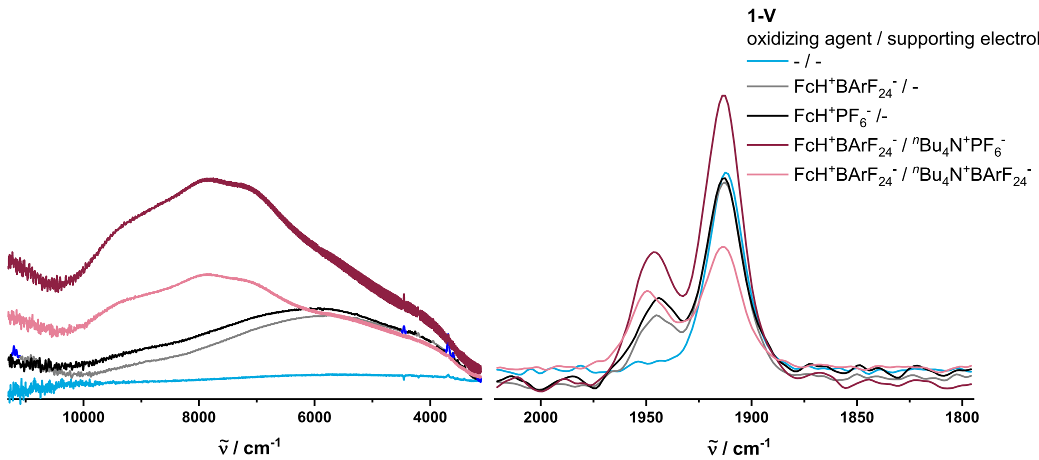

Figure 8. (left) IR/NIR and (right) IR spectra in the region of the $\tilde{\nu}$(CO) bands of neutral **1-V** (blue line) and after chemical oxidation with 0.2 equiv of $FcH^+BArF_{24}^-$ or $FcH^+PF_6^-$ in the absence (gray and black lines) or presence (red and purple lines) of 0.2 M $^nBu_4N^+BArF_{24}^-$ or $^nBu_4N^+PF_6^-$, measured in CH_2Cl_2.

do not differ to a noticeable extent from those of their neutral and two-electron-oxidized forms. The same also holds true for the [**2-A**]$^{0/2+/4+}$ redox series. Reconstruction of the spectra of the MV cations by the procedure described in the Supporting Information provides a pattern of two Ru(CO) bands for [**1-V**]$^{•+}$. The CO band at lower energy appears to be shifted by ca. 2 cm^{-1} with respect to **1-V**, while no shift is observed for the band at higher energy with respect to [**1-V**]$^{2+}$ or for the two CO bands of [**1-A**]$^{•+}$ and [**2-A**]$^{••2+}$ with respect to the neutral or di/tetraoxidized forms (Table 3).

Traversing the first, composite oxidation wave of the complexes also gives rise to distinct changes in the UV/vis/NIR spectra. The results of SEC experiments on **1-V** are shown in Figure 6, and those for **1-A** and **2-A** can be found in Figures S34 and S35. The most obvious change is the continuous growth of an intense, structured absorption that spreads from ca. 800 to 1700 nm. An additional absorption at even lower energy, extending beyond the low-energy limit of the NIR detector, and an intermittent band at 707 nm in the case of **1-V** mark this process as an overall two-step oxidation that proceeds over a defined intermediate with a distinct electronic structure. The intensities of the features characteristic of the intermediate radical cation first increase, pass through a maximum, and then decrease during later stages of the electrolysis, where they either bleach completely or give way to a new absorption at 611 nm. We note that the spectra collected after this point show isosbestic points at 1680 and 790 nm (Figure 6, right panel), whereas a continuous increase in absorbance is found at these wavelengths during the earlier stages (Figure 6, left panel). The NIR feature at lowest energy is identical to the low-energy tail at 4000−6000 cm^{-1} observed in the IR/NIR spectra (see Figures S30−S32).

The spectrum with the highest intensities of the spectroscopic features specific to the respective MV radical cation was used to emulate the UV/vis/NIR spectra of intermediates [**1-V**]$^{•+}$, [**1-A**]$^{•+}$, and [**2-A**]$^{••2+}$ with consideration of the comproportionation equilibrium, applying the procedure described in the Supporting Information. The resultant data are shown in Figure 7 alongside those of the neutral and the di- or tetraoxidized forms and collected in Table 3, while the spectra are provided in Figures S38, S39, and S42. Considering the uncertainties arising from the procedure of spectral reconstruction, we refrain from providing extinction coefficients of the MV complexes. We also note that the initially very intense $\pi \rightarrow \pi^*$ visible band of the neutral complexes suffers a strong loss of absorbance with a concomitant red shift of the remaining absorption. In agreement with previous studies,[60,61,77] one-electron-oxidized metallamacrocycle [**2-A**]$^{•+}$ with one oxidized and one neutral divinylarylene diruthenium entity shows no distinctive spectroscopic signatures for intramolecular electron transfer between these units, due to the insulating character of the dicarboxylato ligands. This matches with the DFT-computed confinement of the unpaired spin density to exclusively one divinylarylene diruthenium subunit of [**2-A**]$^{•+}$ (see Figure S44).

In order to further elucidate the spectroscopic fingerprints of specifically one-electron-oxidized $[\mathbf{1\text{-}A}]^{\bullet+}$ and $[\mathbf{1\text{-}V}]^{\bullet+}$, we treated solutions of the neutral complexes in 1,2-$C_2H_4Cl_2$ with substoichiometric amounts (0.2 equiv) of $FcH^+PF_6^-$ or $FcH^+BArF_{24}^-$ ($BArF_{24}^-$ = $[B\{C_6H_3(CF_3)_2\text{-}3,5\}_4]^-$) as a chemical oxidant and recorded IR/NIR spectra (see Figures 8 and S40). Upon deconvolution, keeping the CO bands of the neutral and dioxidized complexes at their known, fixed positions, no discernible differences in band positions between the Ru(CO) band of $[\mathbf{1\text{-}A}]^{\bullet+}$ at lower energy and that of **1-A** and of the higher-energy Ru(CO) band of $[\mathbf{1\text{-}A}]^{\bullet+}$ with respect to that of $[\mathbf{1\text{-}A}]^{2+}$ were noted (Figure S33). Thus, MV $[\mathbf{1\text{-}A}]^{\bullet+}$ (and, by inference, $[\mathbf{2\text{-}A}]^{\bullet\bullet2+}$) are valence-localized on the vibrational time scale with charge distribution parameters $\Delta\rho$ of or near 0, irrespective of the absence or presence of exogeneous supporting electrolyte (eq 4):

$$\Delta\rho = \frac{[(\tilde{\nu}^{\bullet\bullet2+} - \tilde{\nu}_2^{\bullet+}) + (\tilde{\nu}_1^{\bullet+} - \tilde{\nu}^0)]}{2(\tilde{\nu}^{\bullet\bullet2+} - \tilde{\nu}^0)} \tag{4}$$

where $\tilde{\nu}^{\bullet\bullet2+}$ and $\tilde{\nu}^0$ denote the energies of the Ru(CO) stretching vibrations of the dicationic and neutral complexes, respectively, while $\tilde{\nu}_2^{\bullet+}$ and $\tilde{\nu}_1^{\bullet+}$ are the energies of the higher- and lower-frequency Ru(CO) bands of the radical cation.[24]

However, deconvolution of IR spectra of $[\mathbf{1\text{-}V}]^{\bullet+}$, recorded after adding 0.2 equiv of oxidant, yielded two distinct Ru(CO) bands at 1923 and 1941 cm^{-1} with $BArF_{24}^-$ or at 1921 and 1941 cm^{-1} with PF_6^- as the counteranion (Figure S33). These values differ by 6−8 cm^{-1} from those of neutral **1-V** and $[\mathbf{1\text{-}V}]^{2+}$ (in the absence of a supporting electrolyte, the CO band position of $[\mathbf{1\text{-}V}]^{2+}$ was found at 1948 cm^{-1}). On addition of 0.2 M $^nBu_4N^+PF_6^-$ or $^nBu_4N^+BArF_{24}^-$ to these solutions, the IR bands shifted to 1913 and 1947 cm^{-1}, that is, within error margins, to the same positions as those derived from SEC experiments. It thus seems that an electrolyte influences the extent of the charge distribution in $[\mathbf{1\text{-}V}]^{\bullet+}$. In the presence of supporting electrolyte, localized behavior is seen on the IR time scale. In its absence, $\Delta\rho$ however increases to ca. 0.20, signaling a 20%/80% charge distribution over its molecular halves (eq 4). This matches with previous observations for cationic MV complexes in the presence of higher anion concentrations.[84] While medium effects on the thermodynamic stabilities of the intermediate MV state are well-documented,[85−87] the present results are a rare demonstration of electrolyte effects on the degree of electronic coupling in the MV state.

We also compared the NIR spectra of electrochemically oxidized **1-V** and **1-A** (i.e., those recorded in the presence of a large excess of supporting electrolyte) with those obtained after adding 0.2 equiv of $FcH^+PF_6^-$ or $FcH^+BArF_{24}^-$ as a chemical oxidant in the absence of an additional electrolyte. The results of these studies are shown in Figures 8, S40, and S41. Again, no changes with respect to the SEC results are observed for **1-A**. However, the shape of the NIR absorption envelope of $[\mathbf{1\text{-}V}]^{\bullet+}$ changed appreciably (Figure 8). Thus, NIR spectra obtained after partial chemical oxidation show an enhanced intensity of the low-energy NIR bands, seen as a tail in SEC experiments, and weaker absorptions for the structured, more intense composite band at higher energy. On adding $^nBu_4N^+PF_6^-$ (0.2 M, the same concentration as for SEC measurements), the NIR band envelope changed and assumed the same shape as obtained in SEC studies. This is another manifestation of the impact of the added electrolyte on charge delocalization in the MV state.

We now enter the discussion of the electronic spectra of the oxidized complexes with the prominent, intense absorption in the NIR at ca. 1200 nm that grows continuously during the stepwise formation of dications $[\mathbf{1\text{-}V}]^{2+}$, $[\mathbf{1\text{-}A}]^{2+}$ and of $[\mathbf{2\text{-}A}]^{4+}$. Such features were also observed in oxidized OPVs, OPEs, and OPV/OPE blends, p-doped PPV polymers,[88−91] and oxidized mononuclear {Ru} complexes with a π-extended arylalkenyl ligand.[3,6,92] Of particular note is the absence of any discernible shift between the one- and two-electron-oxidized forms of **1-A** and **1-V** (the same applies for the two- and four-electron-oxidized forms of **2-A**). This absorption must hence originate from an open-shell (metal−)organic chromophore, whose effective conjugation length is identical for the one- and two-electron-oxidized forms. Twofold oxidation generates a second, identical chromophoric unit and hence results in doubled extinction coefficients. This behavior contrasts with the blue shifts observed en route from singly to doubly oxidized **1-S**, **1-^{V}BTD**, and **1-^{e}BTD** and their 1,4-divinylbiphenylene- and 2,2′-bipyridine-bridged congeners,[1,3,4] whose MV radical cations have fully or partially delocalized electronic ground states.

An identical behavior was noted for diarylamine-capped OPVs with differing numbers of phenylenevinylene repeat units in the bridge. The MV radical cations of the electronically more strongly coupled, shorter congeners show specific low-energy electronic bands that differ from those of the dications. As the bridge lengthens, the charge is progressively confined to only one terminal NAr_3 redox site. At this point, the intervalence charge transfer (IVCT) band becomes weak and shrinks into a low-energy shoulder superimposed on the intense absorption of the open-shell π chromophore, just as we observe it here, or vanishes altogether as the bridge gets even longer.[57,58,93] Close similarities between {Ru}- and NAr_2-terminated OPVs are unsurprising, considering that radical cations $[\{Ru\}{-}(CH{=}CH{-}C_6H_4{-}CH{=}CH)_n{-}NAr_{3-n}]^{\bullet+}$ (n = 1−3), which blend these two motifs, constitute MV systems of Class III or at the Class III/II borderline.[94−96] Comparing Barlow's bis(triarylamine)-capped OPVs and the present diruthenium complexes shows that the point where electronic coupling becomes weak is shifted from an OPV-4 to an OPV-3 bridge with one fewer styryl repeat unit. This points to a slightly higher propensity of a {Ru} entity to localize an electron hole compared to NAr_2.

Seeking further insight into the nature of the electronic excitations in the mixed-valent radical cations and the dications, we resorted to quantum-chemical calculations. Previous work on similarly intricate MV systems has identified the BLYP35 functional as being capable of successfully counterbalancing the inherent tendency of the DFT method to delocalize charge in extended π-conjugated systems by 35% admixture of exact Hartree−Fock exchange.[97,98] When applied to PMe_3 models of the radical cations of the present systems, this functional resulted in symmetrical hole distributions and bridge-based oxidations, which is inconsistent with our IR results. In the case of $[\mathbf{1\text{-}A}]^{\bullet+}$, a starting structure, where the input geometries of the terminal {Ru}−styryl groups were chosen so that one had the metrics of a neutral group and the other had those of an oxidized group, resulted in an unsymmetrical structure and charge distribution. In this localized species, the hole (the β-LUMO) is confined to one molecule half with MO coefficients gradually tapering off from the {Ru}−styryl entity and the outer to the inner styryl moiety. The β-HOMO involves the other half of the molecule in an essentially identical manner. This model is denoted as

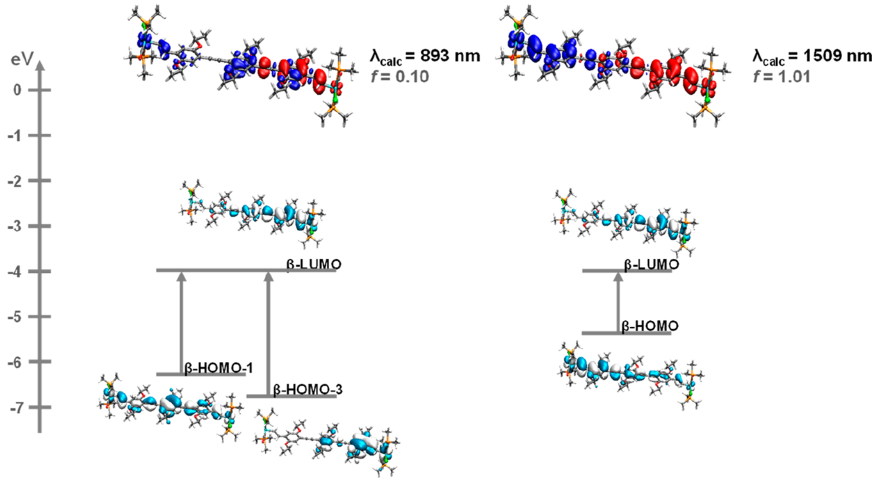

Figure 9. BLYP35/6-31G(d)PCM($ClCH_2-CH_2Cl$)-calculated electronic low-energy transitions of $[\mathbf{1\text{-}A^{Me}}]^{\bullet+d}$ as a desymmetrized model of $[\mathbf{1\text{-}A}]^{\bullet+}$, with the respective donor and acceptor molecular orbitals and the corresponding electron density difference maps (EDDMs) (blue color = electron density decrease and red color = electron density increase).

$[\mathbf{1\text{-}A^{Me}}]^{\bullet+d}$ in the following, where the superscript "d" denotes the "desymmetrized" structure. Applying the same procedure to $[\mathbf{1\text{-}V}]^{\bullet+}$ still resulted in a symmetrical bridge-based β-SOMO.

Two low-energy transitions are predicted for $[\mathbf{1\text{-}A^{Me}}]^{\bullet+d}$: a highly intense band (λ_{calc} = 1509 nm, f = 1.0), which corresponds to the β-HOMO → β-LUMO excitation, and a less intense one at higher energy (λ_{calc} = 893 nm, f = 0.1), which is due to excitation from the lower HOMO−1 and HOMO−3. Both transitions involve charge transfer from one side of the molecule to the other and blend classical IVCT and bridge-to-end-group CT, but they differ with respect to the degree of delocalization of the donor orbital(s) (Figure 9). This is reminiscent of the so-called polaron band in doped OPVs. It seems that our calculations on $[\mathbf{1\text{-}A^{Me}}]^{\bullet+d}$ inverse the energy ordering of the NIR transitions but describe their character adequately. Computed energies for the carbonyl stretching vibrations are 1915 and 1941 cm^{-1}, with displacements of 2 cm^{-1} from the computed band positions in $\mathbf{1\text{-}A^{Me}}$ and $[\mathbf{1\text{-}A^{Me}}]^{2+}$. The overall computed IR band shift of 31 cm^{-1} on twofold oxidation underestimates the experimental value of 45 cm^{-1} but resembles that of 35 cm^{-1} for $[\mathbf{1\text{-}V}]^{0/2+}$. It thus seems that our calculations overestimate bridge contributions to the frontier MOs and that $[\mathbf{1\text{-}A^{Me}}]^{\bullet+d}$ provides a good model for $[\mathbf{1\text{-}V}]^{\bullet+}$. DFT-computed charges on the individual constituents {Ru}-1, bridge, and {Ru}-2 and the differences with respect to $\mathbf{1\text{-}A^{Me}}$ and $[\mathbf{1\text{-}V^{Me}}]^{+}$ are provided in Figures S45 and S46.

In spite of some shortcomings in the quantum-mechanical decriptions of the radical cations, our calculations capture the Vis/NIR spectroscopic features of the dications very well. For the electronic structures of the latter, the singlet, triplet (T), and open-shell singlet (OSS) states need to be considered. Our calculations place the OSS and T states of $[\mathbf{1\text{-}A^{Me}}]^{2+}$ 31 and 28.5 kJ/mol below the closed-shell singlet state. The same energy ordering also applies to $[\mathbf{1\text{-}V^{Me}}]^{2+}$, albeit with smaller energy differences (11.9 and 11 kJ/mol, respectively). Irrespective of the considered spin state, computed spectra of the dications exhibit a highly intense band at 1050−1220 nm for $[\mathbf{1\text{-}A^{Me}}]^{2+}$ or at 1050−1170 nm for $[\mathbf{1\text{-}V^{Me}}]^{2+}$. For the diradical forms with ferro- (T) or antiferromagnetically aligned (OSS) spins, the underlying transition involves the transfer of electron density from the innermost phenyl ring to the peripheral {Ru}−CH═CH acceptor units. For the closed-shell singlets, the direction of charge transfer is reversed. Hence, the diradical and closed-shell singlet forms represent the alternatives of {Ru}−styryl or bridge-based oxidations. The smaller computed energy difference between the closed- and open-shell states of $[\mathbf{1\text{-}V^{Me}}]^{2+}$ is thus consistent with the higher electron-richness of the OPV-3 as compared to the OPE-3 linker.

The computed spectra for the open- and closed-shell states, however, differ in that the former are predicted to exhibit an intense absorption near 550 ($[\mathbf{1\text{-}A^{Me}}]^{2+}$) or 620 nm ($[\mathbf{1\text{-}V^{Me}}]^{2+}$), which has no equivalent in their closed-shell singlet forms (see Figures S50−S52 and S55−S57). Both dications, as well as $[\mathbf{2\text{-}A}]^{4+}$, show two separate bands in this spectral region. Revealingly, the band intensities in alkynyl-bridged $[\mathbf{1\text{-}A}]^{2+}$ and $[\mathbf{2\text{-}A}]^{4+}$ are considerably higher than those in $[\mathbf{1\text{-}V}]^{2+}$, although the computed oscillator strengths of $[\mathbf{1\text{-}A^{Me}}]^{2+}$ and $[\mathbf{1\text{-}V^{Me}}]^{2+}$ are similar. This matches with the computed smaller energetic bias toward the open-shell states and toward {Ru}−styryl compared to entirely bridge-based oxidations in the OPV-3 system. One can speculate that the presence of two separate bands at close energies in this spectral region is due to coexisting OSS and T species.

The lower half-wave potentials and superior stabilities of the higher oxidized forms of **1-V** enabled us to generate these species by chemical oxidation with 3.2 equiv of diacetylferrocenium hexafluoroantimonate and 4.2 equiv of thianthrenium hexafluoroantimonate,[99] respectively, and to record their IR/NIR and UV/vis spectra (see Figure S43). Oxidation to $[\mathbf{1\text{-}V}]^{3+}$ and $[\mathbf{1\text{-}V}]^{4+}$ results in shifts of the CO band to 1966 and 1973 cm^{-1}, respectively. Accompanying changes are also observed in the NIR region. The CT band becomes more structured for $[\mathbf{1\text{-}V}]^{3+}$ and does not change in its intensity, whereas for $[\mathbf{1\text{-}V}]^{4+}$ its intensity is drastically decreased.

EPR Spectroscopy. Electron paramagnetic resonance (EPR) spectroscopy is a powerful tool to probe the distribution of the unpaired spin density in MV compounds. It operates on a time scale of 10^{-7} to 10^{-9} s, which is ca. 3 orders of magnitude slower than that of IR spectroscopy. Hence, the combination of these two methods was repeatedly used to elucidate the rate of intramolecular electron transfer, in particular within the context of one-electron-oxidized bis(triarylamines).[25,54,57,58,93,100−103]

Samples of the one-electron-oxidized species $[\mathbf{1\text{-}V}]^{\bullet+}$ and $[\mathbf{1\text{-}A}]^{\bullet+}$ and two-electron-oxidized $[\mathbf{2\text{-}A}]^{\bullet\bullet 2+}$ were generated by

https://doi.org/10.1021/acs.organomet.3c00337
Organometallics 2023, 42, 3085−3098

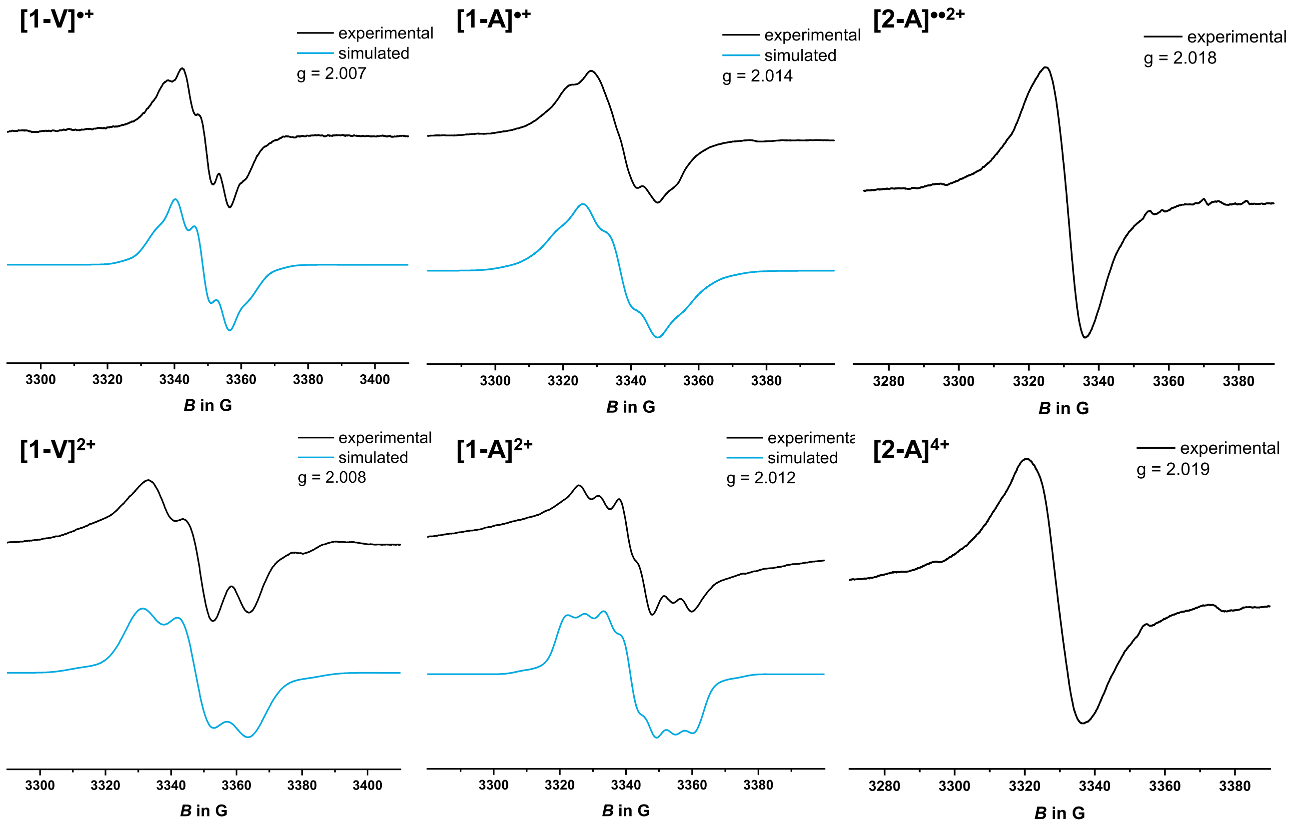

Figure 10. Experimental (black lines) and simulated (blue lines) EPR spectra of compounds, measured at room temperature in CH_2Cl_2.

adding substoichiometric amounts (ca. 0.1 equiv) of $FcH^+PF_6^-$ or $FcH^+BArF_{24}^-$ to the corresponding neutral complexes. $[\mathbf{1\text{-}V}]^{\bullet+}$ and $[\mathbf{1\text{-}A}]^{\bullet+}$ exhibit isotropic signals at g_{iso} values of 2.007 or 2.014, respectively. Most importantly, their EPR spectra show resolved hyperfine splittings with respect to ^{31}P and $^{99/101}Ru$ nuclei (Figure 10). The EPR spectra of both cations are matched by digital simulations[104] assuming identical hfs to four equivalent ^{31}P and two equivalent $^{99/101}Ru$ nuclei. We note, however, that in the case of $[\mathbf{1\text{-}A}]^{\bullet+}$, simulated spectra with two slightly different hfs to two pairs of ^{31}P and two individual $^{99/101}Ru$ nuclei resulted in an equally good fit (see Figure S58). We therefore cannot decide whether this species is fully delocalized on the EPR timescsale or close to this limit. The lack of resolved hfs in $[\mathbf{2\text{-}A}]^{\bullet\bullet2+}$ renders its EPR spectrum uninformative. The larger g_{iso} values of $[\mathbf{1\text{-}A}]^{\bullet+}$ and $[\mathbf{2\text{-}A}]^{\bullet\bullet2+}$ as well as the larger hfs $A(^{99/101}Ru)$ and $A(^{31}P)$ compared to $[\mathbf{1\text{-}V}]^{\bullet+}$ are in line with smaller ligand/higher Ru contributions to the corresponding SOMOs of the alkynylene-bridged complexes.

For diarylamine-terminated OPVs, the breakdown limit of electronic coupling in the MV state coincides with the emergence of a diradical character of the dications.[57,58,93] Samples of the two-electron-oxidized species $[\mathbf{1\text{-}V}]^{2+}$, $[\mathbf{1\text{-}A}]^{2+}$, and of $[\mathbf{2\text{-}A}]^{4+}$ were generated by the addition of 2.1 or 4.2 equiv of acetylferrocenium hexafluoroantimonate to ensure complete oxidation (as was checked by IR/NIR and UV/vis/NIR spectra recorded from these samples) and were found to be EPR-active. $[\mathbf{1\text{-}V}]^{2+}$ and $[\mathbf{1\text{-}A}]^{2+}$ are characterized by resolved hfs to only two ^{31}P nuclei and one $^{99/101}Ru$ nucleus, showing spin confinement to a single {Ru}−CH═CHR site. Values of the hfs constants are approximately twice those for their monocations (Table 4). $[\mathbf{2\text{-}A}]^{4+}$ is also EPR-active with a g_{iso} value of 2.019, yet again does not show resolved hfs.

Table 4. EPR Parameters for $[\mathbf{1\text{-}V}]^{\bullet+}$, $[\mathbf{1\text{-}V}]^{2+}$, $[\mathbf{1\text{-}A}]^{\bullet+}$, $[\mathbf{1\text{-}A}]^{2+}$, $[\mathbf{2\text{-}A}]^{\bullet\bullet2+}$, and $[\mathbf{2\text{-}A}]^{4+}$

		A (G)		
	g_{iso} (20 °C)	^{31}P	$^{99/101}Ru$	^{1}H
$[\mathbf{1\text{-}V}]^{\bullet+}$	2.007	5.7 (4)	3.9 (2)	
$[\mathbf{1\text{-}V}]^{2+}$	2.008	11.4 (2)	7.9 (1)	
$[\mathbf{1\text{-}A}]^{\bullet+}$	2.014	7.7 (4)	6.1 (2)	
$[\mathbf{1\text{-}A}]^{2+}$	2.012	12.5 (2)	11.8 (1)	5.2 (1), 6.2 (1), 4.6 (1), 2.1 (1)[a]
$[\mathbf{2\text{-}A}]^{\bullet\bullet2+}$	2.018			
$[\mathbf{2\text{-}A}]^{4+}$	2.019			

[a] Hyperfine splittings to four separate protons were required in order to arrive at a satisfactory fit between experimental and simulated spectra. According the computed spin densities, the alkenyl protons and the chemically inequivalent protons of the outer phenyl ring are the most likely coupling partners.

CONCLUSIONS

In summary, our present studies on **1-V**, **1-A**, and the derived macrocycle **2-A** expand the series of oligophenylenevinylene (OPV)- and oligophenyleneethynylene (OPE)-bridged diruthenium complexes **1-P**[22] and **1-S**[4] to the next higher OPV-3 congener and its OPV-3/OPE-3 blend. The charge-sensitive CO stretching vibration of the Ru-bonded CO ligands provides us with an indicative spectroscopic handle that probes the local changes of the charge at the {Ru} termini ({Ru} = Ru(CO)-Cl($P^iPr_3)_2$) and the charge density distribution on the fast

https://doi.org/10.1021/acs.organomet.3c00337
Organometallics 2023, 42, 3085−3098

vibrational time scale. Our IR results indicate that $[\mathbf{1\text{-}A}]^{\bullet+}$ and $[\mathbf{2\text{-}A}]^{\bullet\bullet 2+}$ have a localized electronic ground state and place $[\mathbf{1\text{-}V}]^{\bullet+}$ at the Class I/II borderline with a minute fraction of the unipositive charge seeping into the other half of the molecule. Intrinsic valence localization is also indicated by the observation of only a weak intervalence charge transfer (IVCT) band and a strong electronic absorption for an open-shell $[\{Ru\}{-}CH{=}CHAr]^{\bullet+}$ chromophore, whose intensity roughly doubles on twofold oxidation without any apparent band shift. Hence, the cations and dications feature the same spatially confined chromophoric units, whose number simply doubles on oxidation of also the remaining {Ru} terminus. For $[\mathbf{1\text{-}V}]^{\bullet+}$, a considerably larger extent of charge delocalization is, however, noted in the absence of added electrolyte, as seen by the different IR band shifts and an enhanced intensity of the IVCT band. On the slower EPR time scale at room temperature, $[\mathbf{1\text{-}V}]^{\bullet+}$ and $[\mathbf{1\text{-}A}]^{\bullet+}$ are valence-detrapped or close to this limit, as indicated by their hyperfine splitting patterns.

The present diruthenium complexes provide an interesting point of comparison with previously investigated OPVs with diarylamine or tris(polychlorophenyl) radical end caps.[42,57,58,93] The behavior of the present OPV-3-bridged system $[\mathbf{1\text{-}V}]^{\bullet+}$ resembles that of the OPV-4 congeners of its NAr_2-terminated analogs closely. {Ru} entities, while showing close similarities to NAr_2, seemingly have a larger propensity to localize unpaired spin density and likely also an electron hole. This was already indicated by the residual EPR activity of $[\mathbf{1\text{-}P}]^{2+}$[77] and $[\mathbf{1\text{-}S}]^{2+}$ and the $[\mathbf{1\text{-}^{v}BTD_2}]^{2+}$ and $[\mathbf{1\text{-}^{e}BTD_2}]^{2+}$ variants of the latter[1] but becomes particularly manifest in the present study.

■ ASSOCIATED CONTENT

Supporting Information

The Supporting Information is available free of charge at https://pubs.acs.org/doi/10.1021/acs.organomet.3c00337.

Experimental details, procedures, and data (NMR and mass spectra; cyclic and square-wave voltammetry; spectroelectrochemical measurements; IR, EPR, and electronic spectra; quantum-chemical calculations) (PDF)

Cartesian coordinates (XYZ)

■ AUTHOR INFORMATION

Corresponding Author

Rainer F. Winter − *Fachbereich Chemie, Universität Konstanz, 78457 Konstanz, Germany*; orcid.org/0000-0001-8381-0647; Email: Rainer.Winter@uni-konstanz.de

Authors

Franciska S. Gogesch − *Fachbereich Chemie, Universität Konstanz, 78457 Konstanz, Germany*

Sebastian Schwab − *Fachbereich Chemie, Universität Konstanz, 78457 Konstanz, Germany*

Anja Rehse − *Fachbereich Chemie, Universität Konstanz, 78457 Konstanz, Germany*

Michael Linseis − *Fachbereich Chemie, Universität Konstanz, 78457 Konstanz, Germany*

Ananya Baksi − *Fakultät für Chemie und Chemische Biologie, Technische Universität Dortmund, 44227 Dortmund, Germany*

Guido H. Clever − *Fakultät für Chemie und Chemische Biologie, Technische Universität Dortmund, 44227 Dortmund, Germany*; orcid.org/0000-0001-8458-3060

Complete contact information is available at: https://pubs.acs.org/10.1021/acs.organomet.3c00337

Notes

The authors declare no competing financial interest.

■ ACKNOWLEDGMENTS

The authors gratefully acknowledge support of this work by the Deutsche Forschungsgemeinschaft (DFG) through Grants Wi1262/17-1 and INST 40/575-1 FUGG (JUSTUS 2 cluster). We also thank Dr. Mykhailo Azarkh for helpful discussions.

■ REFERENCES

(1) Rotthowe, N.; Zwicker, J.; Winter, R. F. Influence of Quinoidal Distortion on the Electronic Properties of Oxidized Divinylarylene-Bridged Diruthenium Complexes. *Organometallics* **2019**, *38*, 2782−2799.

(2) Man, W. Y.; Xia, J.-L.; Brown, N. J.; Farmer, J. D.; Yufit, D. S.; Howard, J. A. K.; Liu, S. H.; Low, P. J. Spectroscopic and Computational Studies of the Ligand Redox Non-Innocence in Mono- and Binuclear Ruthenium Vinyl Complexes. *Organometallics* **2011**, *30*, 1852−1858.

(3) Linseis, M.; Záliš, S.; Zabel, M.; Winter, R. F. Ruthenium Stilbenyl and Diruthenium Distyrylethene Complexes: Aspects of Electron Delocalization and Electrocatalyzed Isomerization of the Z-Isomer. *J. Am. Chem. Soc.* **2012**, *134*, 16671−16692.

(4) Scheerer, S.; Rotthowe, N.; Abdel-Rahman, O. S.; He, X.; Rigaut, S.; Kvapilová, H.; Záliš, S.; Winter, R. F. Vinyl Ruthenium-Modified Biphenyl and 2,2′-Bipyridines. *Inorg. Chem.* **2015**, *54*, 3387−3402.

(5) Wuttke, E.; Hervault, Y.-M.; Polit, W.; Linseis, M.; Erler, P.; Rigaut, S.; Winter, R. F. Divinylphenylene- and Ethynylvinylphenylene-Bridged Mono-, Di-, and Triruthenium Complexes for Covalent Binding to Gold Electrodes. *Organometallics* **2014**, *33*, 4672−4686.

(6) Wuttke, E.; Fink, D.; Anders, P.; Maria Hoyt, A.-L.; Polit, W.; Linseis, M.; Winter, R. F. Homo- and heterobimetallic 1,4-divinylphenylene- and naphthalene-1,8-divinyl-bridged diruthenium, diosmium and ruthenium osmium complexes. *J. Organomet. Chem.* **2016**, *821*, 4−18.

(7) Pfaff, U.; Hildebrandt, A.; Korb, M.; Oßwald, S.; Linseis, M.; Schreiter, K.; Spange, S.; Winter, R. F.; Lang, H. Electronically Strongly Coupled Divinylheterocyclic-Bridged Diruthenium Complexes. *Chem. - Eur. J.* **2016**, *22*, 783−801.

(8) Mücke, P.; Linseis, M.; Záliš, S.; Winter, R. F. Vinyl-ruthenium entities as markers for intramolecular electron transfer processes. *Inorg. Chim. Acta* **2011**, *374*, 36−50.

(9) Liu, W.-X.; Yan, F.; Qian, S.-L.; Ye, J.-Y.; Liu, X.; Yu, M.-X.; Wu, X.-H.; Le, M.-L.; Zhou, Z.-Y.; Liu, S.-H.; Low, P. J.; Jin, S. Electronic Structures of Divinylchalcogenophene-Bridged Biruthenium Complexes: Exploring Trends from O to Te. *Eur. J. Inorg. Chem.* **2017**, *2017*, 5015−5026.

(10) Wu, X. H.; Jin, S.; Liang, J. H.; Li, Z. Y.; Yu, G.-A.; Liu, S. H. Synthesis, Characterization, and Substituent Effects of Binuclear Ruthenium Vinyl Complexes $[RuCl(CO)(PMe_3)_3]_2(\mu\text{-}CH{=}CH{-}Ar{-}CH{=}CH)$. *Organometallics* **2009**, *28*, 2450−2459.

(11) Wu, X.-H.; Liang, J. H.; Xia, J.-L.; Jin, S.; Yu, G.-A.; Liu, S. H. Bimetallic Ruthenium Complexes: Synthesis, Characterization, and the Effect of Appending Long Carbon Chains to Their Bridges. *Organometallics* **2010**, *29*, 1150−1156.

(12) Tian, L. Y.; Liu, Y. M.; Tian, G.-X.; Wu, X. H.; Li, Z.; Kou, J.-F.; Ou, Y.-P.; Liu, S. H.; Fu, W.-F. Bimetallic ruthenium complexes bridged by divinylphenylene bearing oligo(ethylene glycol)methylether: synthesis, (spectro)electrochemistry and the lithium cation effect. *Dalton Trans.* **2014**, *43*, 4093−4101.

(13) Zhang, J.; Sun, C.-F.; Wu, X.-H.; Zhang, M.-X.; Yin, J.; Yu, G.-A.; Liu, S. H. Bimetallic Ruthenium Vinyl Complexes Bridged by Electronic Substituent Phenylenes: Spectroelectrochemical and Computational Studies. *Int. J. Electrochem. Sci.* **2016**, *11*, 7875−7889.

(14) Jia, G.; Wu, W. F.; Yeung, R. C.; Xia, H. P. Dimeric and polymeric ruthenium complexes with Ru-vinyl linkages. *J. Organomet. Chem.* **1997**, *539*, 53−59.
(15) Xia, H.; Wen, T. B.; Hu, Q. Y.; Wang, X.; Chen, X.; Shek, L. Y.; Williams, I. D.; Wong, K. S.; Wong, G. K. L.; Jia, G. Synthesis and Characterization of Trimetallic Ruthenium and Bimetallic Osmium Complexes with Metal-Vinyl Linkages. *Organometallics* **2005**, *24*, 562−569.
(16) Seetharaman, S. K.; Chung, M.-C.; Englich, U.; Ruhlandt-Senge, K.; Sponsler, M. B. Temperature-Dependent Coordination of Phosphine to Five-Coordinate Alkenylruthenium Complexes. *Inorg. Chem.* **2007**, *46*, 561−567.
(17) Lin, Y.; Yuan, J.; Hu, M.; Cheng, J.; Yin, J.; Jin, S.; Liu, S. H. Syntheses and Properties of Binuclear Ruthenium Vinyl Complexes with Dithienylethene Units as Multifunction Switches. *Organometallics* **2009**, *28*, 6402−6409.
(18) Li, F.; Cheng, J.; Chai, X.; Jin, S.; Wu, X.; Yu, G.-A.; Liu, S. H.; Chen, G. Z. Synthesis, Characterization, and Electrochemical Properties of Diruthenium Complexes Bridged by Anthraquinones. *Organometallics* **2011**, *30*, 1830−1837.
(19) Ou, Y.-P.; Jiang, C.; Wu, D.; Xia, J.; Yin, J.; Jin, S.; Yu, G.-A.; Liu, S. H. Synthesis, Characterization, and Properties of Anthracene-Bridged Bimetallic Ruthenium Vinyl Complexes $[RuCl(CO)(PMe_3)_3]_2(\mu\text{-}CH{=}CH{-}anthracene{-}CH{=}CH)$. *Organometallics* **2011**, *30*, 5763−5770.
(20) Zhang, J.; Ou, Y.; Xu, M.; Sun, C.; Yin, J.; Yu, G.-A.; Liu, S. H. Synthesis and Characterization of Dibenzoheterocycle-Bridged Dinuclear Ruthenium Alkynyl and Vinyl Complexes. *Eur. J. Inorg. Chem.* **2014**, *2014*, 2941−2951.
(21) Kong, D.-D.; Xue, L.-S.; Jang, R.; Liu, B.; Meng, X.-G.; Jin, S.; Ou, Y.-P.; Hao, X.; Liu, S.-H. Conformational Tuning of the Intramolecular Electronic Coupling in Molecular-Wire Biruthenium Complexes Bridged by Biphenyl Derivatives. *Chem. - Eur. J.* **2015**, *21*, 9895−9904.
(22) Maurer, J.; Sarkar, B.; Schwederski, B.; Kaim, W.; Winter, R. F.; Záliš, S. Divinylphenylene-Bridged Diruthenium Complexes Bearing $Ru(CO)Cl(P^iPr_3)_2$ Entities. *Organometallics* **2006**, *25*, 3701−3712.
(23) Robin, M. B.; Day, P. Mixed Valence Chemistry—A Survey and Classification. *Adv. Inorg. Chem. Radiochem.* **1968**, *10*, 247−422.
(24) Stoll, M. E.; Lovelace, S. R.; Geiger, W. E.; Schimanke, H.; Hyla-Kryspin, I.; Gleiter, R. Transannular Effects in Dicobalta-Superphane Complexes on the Mixed-Valence Class II/Class III Interface: Distinguishing between Spin and Charge Delocalization by Electrochemistry, Spectroscopy, and ab Initio Calculations. *J. Am. Chem. Soc.* **1999**, *121*, 9343−9351.
(25) Atwood, C. G.; Geiger, W. E. Investigations of Time-Dependent Delocalization and the Correlation of Carbonyl IR Shifts with $\Delta E_{1/2}$ Values for Hydrocarbon-Linked Class II and Class III Mixed-Valent Complexes. *J. Am. Chem. Soc.* **2000**, *122*, 5477−5485.
(26) Shirakawa, H.; Louis, E. J.; MacDiarmid, A. G.; Chiang, C. K.; Heeger, A. J. Synthesis of electrically conducting organic polymers: halogen derivatives of polyacetylene, $(CH)_x$. *J. Chem. Soc., Chem. Commun.* **1977**, 578.
(27) Chiang, C. K.; Fincher, C. R.; Park, Y. W.; Heeger, A. J.; Shirakawa, H.; Louis, E. J.; Gau, S. C.; MacDiarmid, A. G. Electrical Conductivity in Doped Polyacetylene. *Phys. Rev. Lett.* **1977**, *39*, 1098−1101.
(28) Gagnon, D. R.; Capistran, J. D.; Karasz, F. E.; Lenz, R. W.; Antoun, S. Synthesis, doping, and electrical conductivity of high molecular weight poly(*p*-phenylene vinylene). *Polymer* **1987**, *28*, 567−573.
(29) Gagnon, D. R.; Capistran, J. D.; Karasz, F. E.; Lenz, R. W. Conductivity anisotropy in oriented poly(*p*-Phenylene vinylene). *Polym. Bull.* **1984**, *12*, 293−298.
(30) Davis, W. B.; Svec, W. A.; Ratner, M. A.; Wasielewski, M. R. Molecular-wire behaviour in *p*-phenylenevinylene oligomers. *Nature* **1998**, *396*, 60−63.
(31) *Charge Transport in Organic Semiconductors*; Baessler, H., Koehler, A., Eds.; Springer, 2011. DOI: 10.1007/128_2011_218.
(32) Rauscher, U.; Bässler, H.; Bradley, D. D.; Hennecke, M. Exciton versus band description of the absorption and luminescence spectra in poly(*p*-phenylenevinylene). *Phys. Rev. B* **1990**, *42*, 9830−9836.
(33) Bässler, H.; Deußen, M.; Heun, S.; Lemmer, U.; Mahrt, R. F. Spectroscopy of Conjugated Polymers. *Z. Phys. Chem.* **1994**, *184*, 233−252.
(34) Lee, T.-W.; Park, O. O. The Effect of Different Heat Treatments on the Luminescence Efficiency of Polymer Light-Emitting Diodes. *Adv. Mater.* **2000**, *12*, 801−804.
(35) Hertel, D.; Setayesh, S.; Nothofer, H. G.; Scherf, U.; Müllen, K.; Bässler, H. Phosphorescence in Conjugated Poly(para-phenylene)-Derivatives. *Adv. Mater.* **2001**, *13*, 65−70.
(36) Narwark, O.; Meskers, S.; Peetz, R.; Thorn-Csányi, E.; Bässler, H. Spectroscopic characterization of *p*-phenylene vinylene (PV) oligomers. Part I: A homologous series of 2,5-diheptyloxy substituted PV-oligomers. *Chem. Phys.* **2003**, *294*, 1−15.
(37) Liao, L.; Ding, L.; Karasz, F. E.; Pang, Y. Blue-emitting poly(1,3-phenylenevinylene) derivatives: Effect of substitution patterns on optical properties. *J. Polym. Sci., Part A: Polym. Chem.* **2005**, *43*, 2800−2809.
(38) Burroughes, J. H.; Bradley, D. D. C.; Brown, A. R.; Marks, R. N.; Mackay, K.; Friend, R. H.; Burns, P. L.; Holmes, A. B. Light-emitting diodes based on conjugated polymers. *Nature* **1990**, *347*, 539−541.
(39) Wielopolski, M.; Atienza, C.; Clark, T.; Guldi, D. M.; Martín, N. *p*-Phenyleneethynylene Molecular Wires: Influence of Structure on Photoinduced Electron-Transfer Properties. *Chem. - Eur. J.* **2008**, *14*, 6379−6390.
(40) Turlakov, G.; Arias, E.; Moggio, I.; Rodríguez, G.; Ziolo, R. F.; Rodríguez-Fernández, O. S.; Mikhaylov, A.; Uudsemaa, M.; Cooper, T.; Rebane, A. Photophysical and Electrochemical Properties of Push-Pull Oligo(ferrocenyl-phenyleneethynylene)s: Supramolecular Orders in Molecular Films. *Langmuir* **2022**, *38*, 4077−4089.
(41) Lu, Q.; Yao, C.; Wang, X.; Wang, F. Enhancing Molecular Conductance of Oligo(*p*-phenylene ethynylene)s by Incorporating Ferrocene into Their Backbones. *J. Phys. Chem. C* **2012**, *116*, 17853−17861.
(42) Lloveras, V.; Vidal-Gancedo, J.; Figueira-Duarte, T. M.; Nierengarten, J.-F.; Novoa, J. J.; Mota, F.; Ventosa, N.; Rovira, C.; Veciana, J. Tunneling versus Hopping in Mixed-Valence Oligo-*p*-phenylenevinylene Polychlorinated Bis(triphenylmethyl) Radical Anions. *J. Am. Chem. Soc.* **2011**, *133*, 5818−5833.
(43) Castellano, M.; Fortea-Pérez, F. R.; Bentama, A.; Stiriba, S.-E.; Julve, M.; Lloret, F.; de Munno, G.; Armentano, D.; Li, Y.; Ruiz-García, R.; Cano, J. Dicopper(II) Metallacyclophanes with Oligo(*p*-phenylene-ethynylene) Spacers: Experimental Foundations and Theoretical Predictions on Potential Molecular Magnetic Wires. *Inorg. Chem.* **2013**, *52*, 7645−7657.
(44) Zhou, C.-Z.; Liu, T.; Xu, J.-M.; Chen, Z.-K. Synthesis, Characterization, and Physical Properties of Monodisperse Oligo(*p*-phenyleneethynylene)s. *Macromolecules* **2003**, *36*, 1457−1464.
(45) Atienza, C.; Martín, N.; Wielopolski, M.; Haworth, N.; Clark, T.; Guldi, D. M. Tuning electron transfer through *p*-phenyleneethynylene molecular wires. *Chem. Commun.* **2006**, 3202−3204.
(46) Zhao, X.; Huang, C.; Gulcur, M.; Batsanov, A. S.; Baghernejad, M.; Hong, W.; Bryce, M. R.; Wandlowski, T. Oligo-(aryleneethynylene)s with Terminal Pyridyl Groups: Synthesis and Length Dependence of the Tunneling-to-Hopping Transition of Single-Molecule Conductances. *Chem. Mater.* **2013**, *25*, 4340−4347.
(47) Su, T. A.; Neupane, M.; Steigerwald, M. L.; Venkataraman, L.; Nuckolls, C. Chemical principles of single-molecule electronics. *Nat. Rev. Mater.* **2016**, *1*, 16002.
(48) *Molecular Electronics: An Introduction to Theory and Experiment*, 2nd ed.; Scheer, E., Cuevas, J. C., Eds.; World Scientific Series in Nanoscience and Nanotechnology, Vol. *15*; World Scientific, 2017. DOI: 10.1142/10598.
(49) Liu, H.; Wang, N.; Zhao, J.; Guo, Y.; Yin, X.; Boey, F. Y. C.; Zhang, H. Length-Dependent Conductance of Molecular Wires and Contact Resistance in Metal-Molecule-Metal Junctions. *ChemPhysChem* **2008**, *9*, 1416−1424.

(50) Davis, W. B.; Ratner, M. A.; Wasielewski, M. R. Conformational Gating of Long Distance Electron Transfer through Wire-like Bridges in Donor-Bridge-Acceptor Molecules. *J. Am. Chem. Soc.* **2001**, *123*, 7877−7886.

(51) Lu, Q.; Liu, K.; Zhang, H.; Du, Z.; Wang, X.; Wang, F. From Tunneling to Hopping: A Comprehensive Investigation of Charge Transport Mechanism in Molecular Junctions Based on Oligo(*p*-phenylene ethynylene)s. *ACS Nano* **2009**, *3*, 3861−3868.

(52) Kaliginedi, V.; Moreno-García, P.; Valkenier, H.; Hong, W.; García-Suárez, V. M.; Buiter, P.; Otten, J. L. H.; Hummelen, J. C.; Lambert, C. J.; Wandlowski, T. Correlations between Molecular Structure and Single-Junction Conductance: A Case Study with Oligo(phenylene-ethynylene)-Type Wires. *J. Am. Chem. Soc.* **2012**, *134*, 5262−5275.

(53) Hong, W.; Li, H.; Liu, S.-X.; Fu, Y.; Li, J.; Kaliginedi, V.; Decurtins, S.; Wandlowski, T. Trimethylsilyl-Terminated Oligo-(phenylene ethynylene)s: An Approach to Single-Molecule Junctions with Covalent Au-C σ-Bonds. *J. Am. Chem. Soc.* **2012**, *134*, 19425−19431.

(54) Lancaster, K.; Odom, S. A.; Jones, S. C.; Thayumanavan, S.; Marder, S. R.; Brédas, J.-L.; Coropceanu, V.; Barlow, S. Intramolecular Electron-Transfer Rates in Mixed-Valence Triarylamines: Measurement by Variable-Temperature ESR Spectroscopy and Comparison with Optical Data. *J. Am. Chem. Soc.* **2009**, *131*, 1717−1723.

(55) Giacalone, F.; Segura, J. L.; Martín, N.; Ramey, J.; Guldi, D. M. Probing Molecular Wires: Synthesis, Structural, and Electronic Study of Donor-Acceptor Assemblies Exhibiting Long-Range Electron Transfer. *Chem. - Eur. J.* **2005**, *11*, 4819−4834.

(56) Peeters, E.; van Hal, P. A.; Knol, J.; Brabec, C. J.; Sariciftci, N. S.; Hummelen, J. C.; Janssen, R. A. J. Synthesis, Photophysical Properties, and Photovoltaic Devices of Oligo(-phenylene vinylene)-fullerene Dyads. *J. Phys. Chem. B* **2000**, *104*, 10174−10190.

(57) Barlow, S.; Risko, C.; Chung, S.-J.; Tucker, N. M.; Coropceanu, V.; Jones, S. C.; Levi, Z.; Brédas, J.-L.; Marder, S. R. Intervalence Transitions in the Mixed-Valence Monocations of Bis(triarylamines) Linked with Vinylene and Phenylene-Vinylene Bridges. *J. Am. Chem. Soc.* **2005**, *127*, 16900−16911.

(58) Barlow, S.; Risko, C.; Odom, S. A.; Zheng, S.; Coropceanu, V.; Beverina, L.; Brédas, J.-L.; Marder, S. R. Tuning Delocalization in the Radical Cations of 1,4-Bis[4-(diarylamino)styryl]benzenes, 2,5-Bis[4-(diarylamino)styryl]thiophenes, and 2,5-Bis[4-(diarylamino)styryl]-pyrroles through Substituent Effects. *J. Am. Chem. Soc.* **2012**, *134*, 10146−10155.

(59) Werner, H.; Esteruelas, M. A.; Otto, H. Insertion reactions of the 16-electron complexes $MHCl(CO)[P(CHMe_2)_3]_2$ (M = Ru, Os) with alkynes. The x-ray crystal structure of $[(E)\text{-}PhCH{:}CHOs(Cl)(CO)\text{-}[P(CHMe_2)_3]_2$. *Organometallics* **1986**, *5*, 2295−2299.

(60) Anders, P.; Rapp, M.; Linseis, M.; Winter, R. Tetraruthenium Metallamacrocycles with Potentially Coordinating Appended Functionalities. *Inorganics* **2018**, *6*, 73−94.

(61) Fink, D.; Orth, N.; Ebel, V.; Gogesch, F. S.; Staiger, A.; Linseis, M.; Ivanović-Burmazović, I.; Winter, R. F. Self-Assembled Redox-Active Tetraruthenium Macrocycles with Large Intracyclic Cavities. *Organometallics* **2020**, *39*, 1861−1880.

(62) Fink, D.; Linseis, M.; Winter, R. F. Constitutional Isomers of Macrocyclic Tetraruthenium Complexes with Vastly Different Spectroscopic and Electrochemical Properties. *Organometallics* **2018**, *37*, 1817−1820.

(63) Stalmach, U.; Kolshorn, H.; Brehm, I.; Meier, H. Monodisperse Dialkoxy-Substituted Oligo(phenyleneethenylene)s. *Eur. J. Org. Chem.* **1996**, *1996*, 1449−1456.

(64) Ndayikengurukiye, H.; Jacobs, S.; Tachelet, W.; van der Looy, J.; Pollaris, A.; Geise, H. J.; Claeys, M.; Kauffmann, J. M.; Janietz, S. Alkoxylated *p*-phenylenevinylene oligomers: Synthesis and spectroscopic and electrochemical properties. *Tetrahedron* **1997**, *53*, 13811−13828.

(65) Schenning, A. P. H. J.; Tsipis, A. C.; Meskers, S. C. J.; Beljonne, D.; Meijer, E. W.; Brédas, J. L. Electronic Structure and Optical Properties of Mixed Phenylene Vinylene/Phenylene Ethynylene Conjugated Oligomers. *Chem. Mater.* **2002**, *14*, 1362−1368.

(66) Detert, H.; Sugiono, E. The synthesis and condensation of oligo(phenylenevinylene)s with alkoxysilyl end groups. *Macromol. Symp.* **2002**, *181*, 39−46.

(67) Detert, H.; Sadovski, O. Triarylamines connected via phenylenevinylene segments. *Synth. Met.* **2003**, *138*, 185−188.

(68) Frisch, M. J.; Trucks, G. W.; Schlegel, H. B.; Scuseria, G. E.; Robb, M. A.; Cheeseman, J. R.; Scalmani, G.; Barone, V.; Mennucci, B.; Petersson, G. A.; Nakatsuji, H.; Caricato, M.; Li, X.; Hratchian, H. P.; Izmaylov, A. F.; Bloino, J.; Zheng, G.; Sonnenberg, J. L.; Hada, M.; Ehara, M.; Toyota, K.; Fukuda, R.; Hasegawa, J.; Ishida, M.; Nakajima, T.; Honda, Y.; Kitao, O.; Nakai, H.; Vreven, T.; Montgomery, J. A., Jr.; Peralta, J. E.; Ogliaro, F.; Bearpark, M.; Heyd, J. J.; Brothers, E.; Kudin, K. N.; Staroverov, V. N.; Kobayashi, R.; Normand, J.; Raghavachari, K.; Rendell, A.; Burant, J. C.; Iyengar, S. S.; Tomasi, J.; Cossi, M.; Rega, N.; Millam, J. M.; Klene, M.; Knox, J. E.; Cross, J. B.; Bakken, V.; Adamo, C.; Jaramillo, J.; Gomperts, R.; Stratmann, R. E.; Yazyev, O.; Austin, A. J.; Cammi, R.; Pomelli, C.; Ochterski, J. W.; Martin, R. L.; Morokuma, K.; Zakrzewski, V. G.; Voth, G. A.; Salvador, P.; Dannenberg, J. J.; Dapprich, S.; Daniels, A. D.; Farkas, Ö.; Foresman, J. B.; Ortiz, J. V.; Cioslowski, J.; Fox, D. J. *Gaussian 09*, rev. D.01; Gaussian, Inc.: Wallingford, CT, 2009.

(69) Hansch, C.; Leo, A.; Taft, R. W. A survey of Hammett substituent constants and resonance and field parameters. *Chem. Rev.* **1991**, *91*, 165−195.

(70) Egbe, D. A. M.; Nguyen, L. H.; Hoppe, H.; Mühlbacher, D.; Sariciftci, N. S. Side Chain Influence on Electrochemical and Photovoltaic Properties of Yne-Containing Poly(phenylene vinylene)s. *Macromol. Rapid Commun.* **2005**, *26*, 1389−1394.

(71) Shi, C.; Yang, K.; Cao, Y. Synthesis and Optical Properties of Soluble Conjugated Poly(*p*-diethynylbenzene)s. *Synth. Met.* **2005**, *154*, 121−124.

(72) Gebhardt, V.; Bacher, A.; Thelakkat, M.; Stalmach, U.; Meier, H.; Schmidt, H.-W.; Haarer, D. Electroluminescent Behavior of a Homologous Series of Phenylenevinylene Oligomers. *Adv. Mater.* **1999**, *11*, 119−123.

(73) Zou, Y.; Tan, Z.; Huo, L.; Li, Y. A phenylenevinylene-thiophene-phenyleneethynylene copolymer: synthesis, characterization, and photovoltaic properties. *Polym. Adv. Technol.* **2008**, *19*, 865−871.

(74) Rudolph, M.; Feldberg, S. W. *DigiSim* ver. 3.03; Bioanalytical Systems, Inc., 1994.

(75) Ketter, J. B.; Forry, S. P.; Wightman, R. M.; Feldberg, S. W. The Electrochemical Society Use of DigiSim to Model Cyclic Voltammetric and Photonic Responses in Electrogenerated Chemiluminescent Systems. *Electrochem. Solid.-State Lett.* **2004**, *7*, E18−E22.

(76) Kushmerick, J. G.; Holt, D. B.; Pollack, S. K.; Ratner, M. A.; Yang, J. C.; Schull, T. L.; Naciri, J.; Moore, M. H.; Shashidhar, R. Effect of bond-length alternation in molecular wires. *J. Am. Chem. Soc.* **2002**, *124*, 10654−10655.

(77) Scheerer, S.; Linseis, M.; Wuttke, E.; Weickert, S.; Drescher, M.; Tröppner, O.; Ivanović-Burmazović, I.; Irmler, A.; Pauly, F.; Winter, R. F. Redox-Active Tetraruthenium Macrocycles Built from 1,4-Divinylphenylene-Bridged Diruthenium Complexes. *Chem. - Eur. J.* **2016**, *22*, 9574−9590.

(78) Fink, D.; Orth, N.; Linseis, M.; Ivanović-Burmazović, I.; Winter, R. F. Ring Size Matters: Polymerization Isomerism in Self-Assembled Redox-Active Tetra- and Hexaruthenium Macrocycles. *Chem. Commun.* **2020**, *56*, 1062−1065.

(79) Helbig, M.; Hörhold, H.-H. Investigation of poly-(arylenevinylene)s, 40. Electrochemical studies on poly(*p*-phenylenevinylene)s. *Makromol. Chem.* **1993**, *194*, 1607−1618.

(80) Heinze, J.; Mortensen, J.; Müllen, K.; Schenk, R. The charge storage mechanism of conducting polymers: a voltammetric study on defined soluble oligomers of the phenylene-vinylene type. *J. Chem. Soc., Chem. Commun.* **1987**, 701−703.

(81) Krejčik, M.; Daněk, M.; Hartl, F. Simple construction of an infrared optically transparent thin-layer electrochemical cell: Applications to the redox reactions of ferrocene, $Mn_2(CO)_{10}$ and Mn-

https://doi.org/10.1021/acs.organomet.3c00337
Organometallics 2023, 42, 3085−3098

$(CO)_3$(3,5-di-*t*-butyl-catecholate)$^-$. *J. Electroanal. Chem.* **1991**, *317*, 179−187.
(82) Connelly, N. G.; Geiger, W. E. Chemical Redox Agents for Organometallic Chemistry. *Chem. Rev.* **1996**, *96*, 877−910.
(83) Sherlock, S. J.; Boyd, D. C.; Moasser, B.; Gladfelter, W. L. Homogeneous catalytic carbonylation of nitroaromatics. 4. Preparation and characterization of ruthenium radical cations. *Inorg. Chem.* **1991**, *30*, 3626−3632.
(84) Fellows, E. A.; Keene, F. R. Influence of Anions on Intervalence Charge Transfer (IVCT) in Mixed-Valence Dinuclear Complexes. *J. Phys. Chem. B* **2007**, *111*, 6667−6675.
(85) Barrière, F.; Camire, N.; Geiger, W. E.; Mueller-Westerhoff, U. T.; Sanders, R. Use of Medium Effects to Tune the $\Delta E_{1/2}$ Values of Bimetallic and Oligometallic Compounds. *J. Am. Chem. Soc.* **2002**, *124*, 7262−7263.
(86) Barrière, F.; Geiger, W. E. Use of Weakly Coordinating Anions to Develop an Integrated Approach to the Tuning of $\Delta E_{1/2}$ Values by Medium Effects. *J. Am. Chem. Soc.* **2006**, *128*, 3980−3989.
(87) D'Alessandro, D. M.; Keene, F. R. A cautionary warning on the use of electrochemical measurements to calculate comproportionation constants for mixed-valence compounds. *Dalton Trans.* **2004**, 3950−3954.
(88) Deussen, M.; Bässler, H. Anion and cation absorption spectra of conjugated oligomers and polymers. *Chem. Phys.* **1992**, *164*, 247−257.
(89) van Hal, P. A.; Beckers, E. H.; Peeters, E.; Apperloo, J. J.; Janssen, R. A. Photoinduced intermolecular electron transfer between oligo(*p*-phenylene vinylene)s and *N*-methylfulleropyrrolidine in a polar solvent. *Chem. Phys. Lett.* **2000**, *328*, 403−408.
(90) Grozema, F. C.; Candeias, L. P.; Swart, M.; van Duijnen, P. T.; Wildeman, J.; Hadziioanou, G.; Siebbeles, L. D. A.; Warman, J. M. Theoretical and experimental studies of the opto-electronic properties of positively charged oligo(phenylene vinylene)s: Effects of chain length and alkoxy substitution. *J. Chem. Phys.* **2002**, *117*, 11366−11378.
(91) Holt, A. L.; Leger, J. M.; Carter, S. A. Electrochemical and optical characterization of *p*- and *n*-doped poly[2-methoxy-5-(2-ethylhexyloxy)-1,4-phenylenevinylene]. *J. Chem. Phys.* **2005**, *123*, 044704.
(92) Maurer, J.; Linseis, M.; Sarkar, B.; Schwederski, B.; Niemeyer, M.; Kaim, W.; Zalis, S.; Anson, C.; Zabel, M.; Winter, R. F. Ruthenium Complexes with Vinyl, Styryl, and Vinylpyrenyl Ligands: A Case of Non-innocence in Organometallic Chemistry. *J. Am. Chem. Soc.* **2008**, *130*, 259−268.
(93) Burrezo, P. M.; Lin, N.-T.; Nakabayashi, K.; Ohkoshi, S.; Calzado, E. M.; Boj, P. G.; Díaz García, M. A.; Franco, C.; Rovira, C.; Veciana, J.; Moos, M.; Lambert, C.; López Navarrete, J. T.; Tsuji, H.; Nakamura, E.; Casado, J. Bis(aminoaryl) Carbon-Bridged Oligo-(phenylenevinylene)s Expand the Limits of Electronic Couplings. *Angew. Chem.* **2017**, *129*, 2944−2948.
(94) Polit, W.; Exner, T.; Wuttke, E.; Winter, R. F. Vinylruthenium-triarylamine conjugates as electroswitchable polyelectrochromic NIR dyes. *BioInorg. React. Mech.* **2012**, *8*, 85−105.
(95) Hassenrück, C.; Winter, R. F. Manipulation and Assessment of Charge and Spin Delocalization in Mixed-Valent Triarylamine-Vinylruthenium Conjugates. *Inorg. Chem.* **2017**, *56*, 13517−13529.
(96) Breimaier, S.; Fröhlich, N.; Herberger, J.; Linseis, M.; Kivala, M.; Winter, R. F. Charge and Spin Delocalization in Mixed-Valent Vinylruthenium-Triarylamine-Conjugates with Planarized Triarylamines. *Organometallics* **2022**, *41*, 532−546.
(97) Renz, M.; Theilacker, K.; Lambert, C.; Kaupp, M. A Reliable Quantum-Chemical Protocol for the Characterization of Organic Mixed-Valence Compounds. *J. Am. Chem. Soc.* **2009**, *131*, 16292−16302.
(98) Kaupp, M.; Renz, M.; Parthey, M.; Stolte, M.; Würthner, F.; Lambert, C. Computational and spectroscopic studies of organic mixed-valence compounds: where is the charge? *Phys. Chem. Chem. Phys.* **2011**, *13*, 16973−16986.
(99) Lee, W. K.; Liu, B.; Park, C. W.; Shine, H. J.; Guzman-Jimenez, I. Y.; Whitmire, K. H. Addition of Thianthrene Cation Radical to Cycloalkenes. An Unexpected Monoadduct. *J. Org. Chem.* **1999**, *64*, 9206−9210.
(100) Kattnig, D. R.; Mladenova, B.; Grampp, G.; Kaiser, C.; Heckmann, A.; Lambert, C. Electron Paramagnetic Resonance Spectroscopy of Bis(triarylamine) Paracyclophanes as Model Compounds for the Intermolecular Charge-Transfer in Solid State Materials for Optoelectronic Applications. *J. Phys. Chem. C* **2009**, *113*, 2983−2995.
(101) Schäfer, J.; Holzapfel, M.; Mladenova, B.; Kattnig, D.; Krummenacher, I.; Braunschweig, H.; Grampp, G.; Lambert, C. Hole Transfer Processes in meta- and para-Conjugated Mixed Valence Compounds: Unforeseen Effects of Bridge Substituents and Solvent Dynamics. *J. Am. Chem. Soc.* **2017**, *139*, 6200−6209.
(102) Abdel-Rahman, O. S.; Jan, M. T.; Oßwald, S.; Winter, R. F. Polyelectrochromism and electronic coupling in vinylruthenium-modified carbazoles. *J. Organomet. Chem.* **2017**, *849*−*850*, 98−116.
(103) Atwood, C. G.; Geiger, W. E.; Rheingold, A. L. Structural consequences of electron-transfer reactions. 26. Evidence for time-dependent valence detrapping in a mixed-valent dimanganese fulvalenyl cation. *J. Am. Chem. Soc.* **1993**, *115*, 5310−5311.
(104) Stoll, S.; Schweiger, A. EasySpin, a comprehensive software package for spectral simulation and analysis in EPR. *J. Magn. Reson.* **2006**, *178*, 42−55.

https://doi.org/10.1021/acs.organomet.3c00337
Organometallics 2023, 42, 3085−3098